https://doi.org/10.5194/egusphere-2025-1229
Preprint. Discussion started: 13 May 2025

Evaluation of a coupled ocean and sea-ice model (MOM6-NEP10k) over the Bering Sea and its sensitivity to turbulence decay scales

Vivek Seelanki [1,2], Wei Cheng[2], Phyllis J. Stabeno[2], Albert J. Hermann[1,2], Elizabeth J. Drenkard[3], Charles A. Stock[3], Katherine Hedstrom[4]

[1]CICOES, University of Washington, Seattle, WA, 98195, USA
[2]NOAA OAR PMEL, Seattle, WA, 98115, USA
[3]NOAA OAR GFDL, Princeton, NJ, 08540, USA
[4]University of Alaska Fairbanks, Fairbanks, AK, 99775, USA

Correspondence to: Vivek Seelanki (viveklp@uw.edu)

Abstract. Understanding and predicting the ocean environment and marine ecosystem status depends on accurate representations of regional ocean dynamics. Recently, the Modular Ocean Model version 6 (MOM6) has been configured to span the Northeast Pacific Ocean from Baja California to the Chukchi Sea (MOM6-NEP). In this study we present a physical hindcast (1993-2018) simulation of MOM6-NEP where it is coupled to a thermodynamic-dynamic sea-ice module and includes tides. We evaluate performance of this model in the Bering Sea. Various model metrics are benchmarked against in-situ mooring data and satellite observations. The simulation captures the general characteristics of Bering Sea dynamics, particularly with respect to seasonal and interannual variability of the middle shelf water mass properties. Modeling of shear induced mixing was found to be critical to the model's ability to reproduce the observed sharp summer thermocline and its depth. The hindcast simulation reproduces the long-term mean timing of sea-ice arrival and retreat in both the northern and southern Bering Sea, with the remaining mild biases primarily occurring in May over the northern shelf - the modeled sea ice tends to retreat earlier (later) in cold (warm) years than observations. This pattern in biases suggests that the melting rate in the model likely lacks the well-known melt-rate dependency on ice property whereby thicker (thinner) ice melts more slowly (quickly). As a result of high skills in reproducing sea ice areal coverage, the interannual variability of the cold pool (the cold-water mass present on the bottom of the Bering Sea shelf in summer) extent is accurately reproduced by the model. Skillful representation of sea ice and cold pool is essential for understanding ecosystem dynamics and successful fisheries management in the Bering Sea. The findings of this study contribute to the development of reliable oceanographic modeling and forecasting of marine ecosystem conditions to support fisheries management decision making.

1 Introduction

The Bering Sea is one of the world's most productive marine ecosystems with abundant populations of fishes, birds, and marine mammals. More than 10% of the world's fish and shellfish and about half of the U.S. commercial seafood harvest come from these ecosystems (Wang et al., 2009, 2013). In addition, subsistence harvests are important for the livelihoods and cultures of

https://doi.org/10.5194/egusphere-2025-1229
Preprint. Discussion started: 13 May 2025

many families and communities in Alaska. Each year, approximately 37 million pounds of foods are harvested by rural communities. The significance of the productivity of the Bering Sea extends beyond the United States to the economics of its neighboring countries, including Canada and Russia.

The Bering Sea is a semi-enclosed sea (Fig. 1). To the south, the Aleutian Islands form a porous boundary between the Gulf of Alaska and the Bering Sea, and to the north, the Bering Sea is connected to the Arctic Ocean via the narrow (~85 km), shallow (30 - 50 m) Bering Strait, which is the only source of Pacific water into the Arctic Ocean. The Bering Sea is divided almost equally between the broad (~500 km wide) eastern shelf and the deep basin. The eastern Bering Sea shelf is bisected north-south at ~60°N, with the southern shelf being more pelagic and the northern shelf more benthic (Stabeno et al., 2012). There are three cross shelf domains that are evident in summer: the coastal or inner shelf domain (0 - 50 m deep), which is only weakly stratified; the middle domain (50 - 100 m), which is strongly stratified with a well-mixed surface layer and tidally mixed bottom layer; and the outer domain (100 - 180 m), which is more oceanic in its vertical structure (Coachman, 1986; Stabeno, 1999). These domains are more distinct on the southern shelf where the tidal velocity is approximately twice as strong compared to the northern shelf, but the domains exist from the Alaska Peninsula to St. Lawrence Island, ~1000 km to the north.

https://doi.org/10.5194/egusphere-2025-1229
Preprint. Discussion started: 13 May 2025

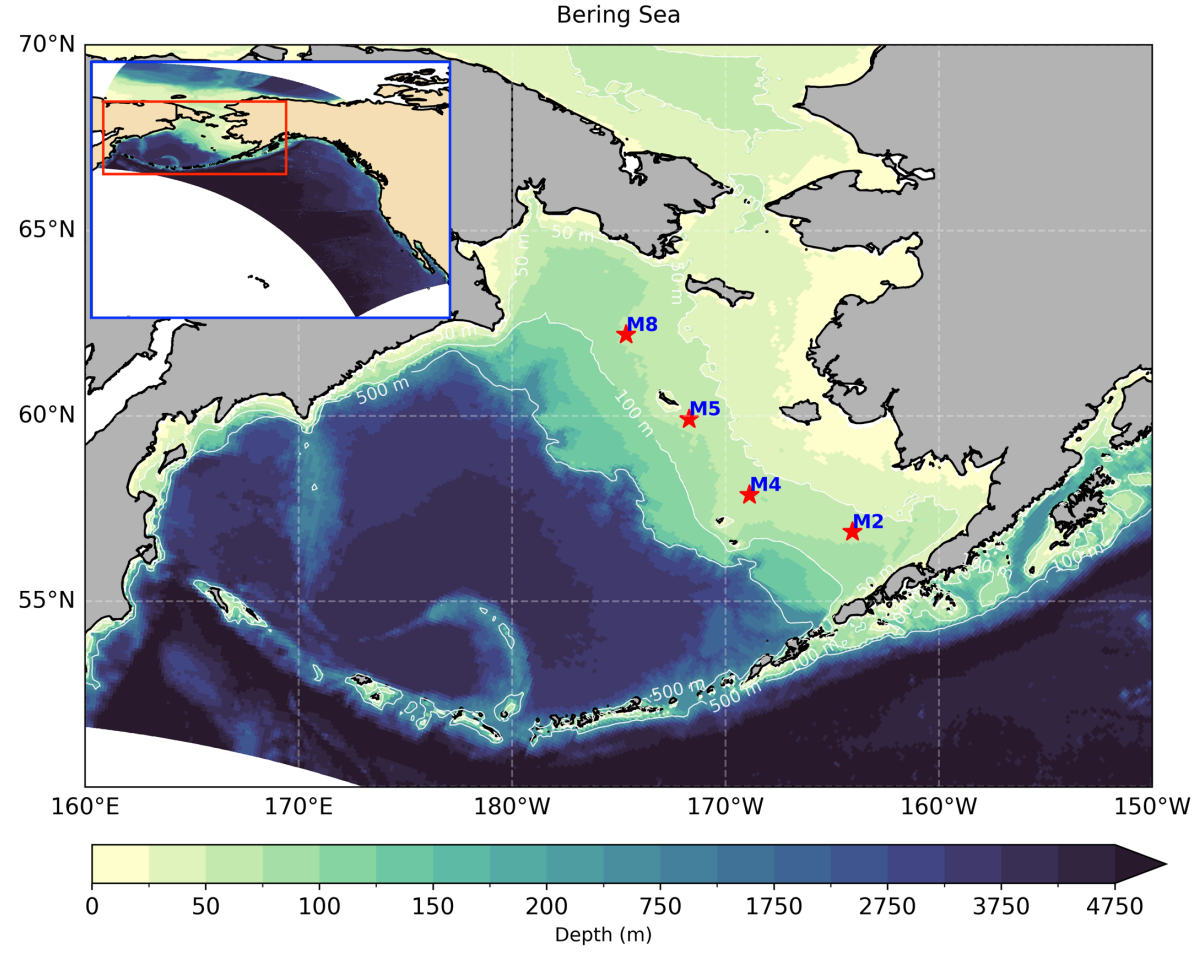

Figure 1: Study region (Bering Sea) with locations of biophysical moorings M2, M4, M5 and M8 shown by the red stars. The entire model domain is shown in the upper left-hand corner.

Well defined flow patterns exist in both the basin and over the shelf (Fig. 2a). Gulf of Alaska water enters the Bering Sea through the eastern and central Aleutian Passes and exits into the Gulf of Alaska through the western passes. Flow on the eastern shelf is generally northward, in several well-defined currents (Fig. 2a). Bering Sea water also flows northward through Bering Strait into the Arctic Ocean. The Bering Sea circulation has strong seasonal variability, driven by the Aleutian Low and Siberian High atmospheric pressure systems (Danielson et al., 2011; Frey et al., 2015; Zhang et al., 2010). The northeasterly winds in winter carry cold air from the Arctic, resulting in the formation of sea ice. In the summer, the southwesterly wind brings warm air from the south to the Bering Sea, which contributes to sea-ice retreat and melting (Woodgate et al., 2010). Interannual variability of sea ice on the Bering Sea shelf is also influenced by fluctuations of ocean

https://doi.org/10.5194/egusphere-2025-1229
Preprint. Discussion started: 13 May 2025

transport and the associated heat and freshwater fluxes through the porous Aleutian Islands (Stabeno and Cheng, in prep) and Bering Strait (Woodgate et al., 2006; Woodgate et al., 2012). Sea ice is a critical component of the Bering Sea ecosystem. It sets up the "cold pool", a layer of cold (traditionally defined as <2°C) bottom water over the eastern shelf that can persist through the summer. The extent of the cold pool affects species distribution. In addition, the timing of sea-ice melt influences the timing of the spring phytoplankton bloom (Hunt et al., 2002, 2011).

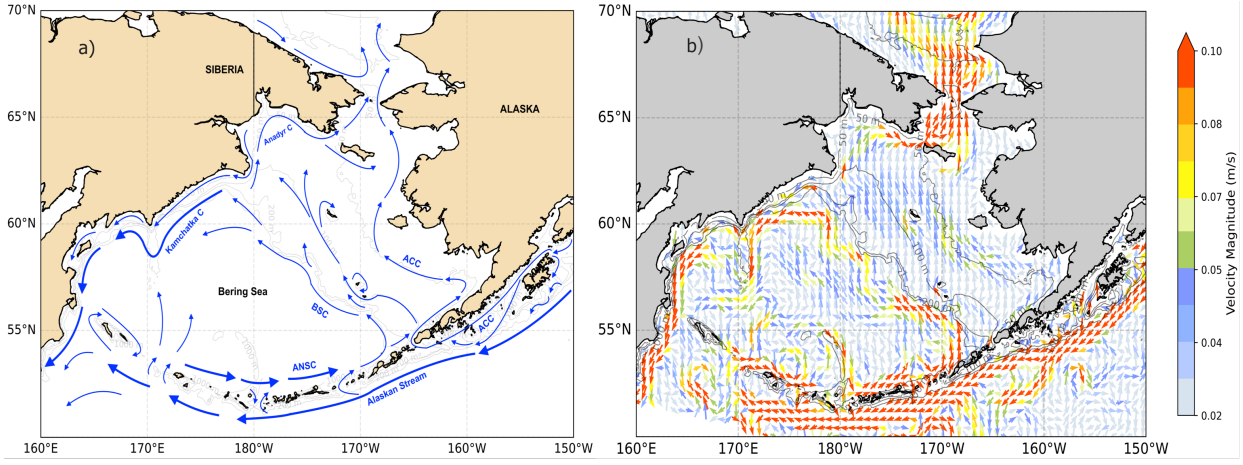

Figure 2: (a) A schematic of the flow patterns in the Bering Sea and along the Aleutian Islands (adapted from Stabeno et al., 1999; 2005). Abbreviations: ANSC is Aleutian North Slope Current; BSC is Bering Slope Current; and the ACC is the Alaskan Coastal Current. (b) Annual mean current in 2016 at 20 meters depth from MOM6-NEP10k. Vectors represent the current direction and color indicates the speed.

Over the past several decades, extensive oceanographic and fisheries observations have been conducted in this rich ecosystem. Measurements include shipboard conductivity-temperature-depth (CTD) casts, biophysical moorings (Stabeno et al., 2023; Cokelet and Stabeno, 1997; Onishi and Ohtani, 1999), shipboard and moored ADCP (Acoustic Doppler Current Profiler) velocity (Cokelet et al., 1996; Stabeno et al., 2016), and satellite-tracked drifters (Stabeno and Reed, 1994). While these observations reveal structure and dynamics of the Bering Sea, they are limited in time and space, providing an incomplete picture of the relationship among physical, chemical and biological processes. Coupled ocean/sea-ice simulations are necessary to gain a better understanding of the Bering Sea and to predict its changes on seasonal, interannual and multidecadal time scales which are driven by natural variability and human activities. These predictions can provide information to help decision makers to better manage marine fisheries and inform local communities who depend on these marine ecosystems.

https://doi.org/10.5194/egusphere-2025-1229
Preprint. Discussion started: 13 May 2025

Recently, a new regional ocean model configuration has been developed stretching from the Baja Peninsula through the Bering Sea and into the Chukchi Sea (Drenkard et al., 2024). It is based on the Modular Ocean Model version 6 (MOM6; (Adcroft et al., 2019), which plays a growing role in regional ocean modeling across NOAA line offices. This configuration, which focuses on the Northeast Pacific (MOM6-NEP), captures numerous fisheries-critical physical and biogeochemical features across the disparate marine ecosystems encompassed by this large domain with fair to high skill. The Bering Sea, however, proved particularly challenging due to its extraordinary range of bathymetric features, dynamic circulation, and atmosphere/ocean/sea-ice interactions. Together with the outsized importance of the Bering Sea ecosystem for commercial and subsistence fisheries, this provides a compelling impetus for a more detailed evaluation of the model performance in this region.

In this paper, we performed hindcasts (using MOM6-NEP) from 1993-2018 under historical atmospheric and oceanic lateral boundary conditions. First, to address excessive shear-driven vertical mixing found in MOM6-NEP default configuration, we implemented a non-dimensional scaling factor to turbulent mixing decay length scale and examined sensitivity of the simulated water mass characteristics to this factor. Using this new scaling factor, we then focused on three components of model output: general circulation; sea-ice timing and extent; and water column stratification. We evaluate this output against long-term bio-physical mooring data (Stabeno et al., 2023), satellite observations (sea surface temperature, sea-ice extent, sea surface height, etc.), and mixed layer depth based on World Ocean Atlas and ARGO dataset. This work supports the NOAA Climate, Ecosystems, and Fisheries Initiative (CEFI) to assist NOAA Fisheries management.

2 Methods and Datasets

2.1 Model Description

MOM6 incorporates many improvements compared to its predecessor, MOM5 (Griffies, 2014), including: the incorporation of the Arbitrary Lagrangian Eulerian (ALE) vertical coordinate (Bleck, 2002; Griffies et al., 2020); the implementation of tracer advection schemes that are more efficient; and state-of-the-art parameterizations of sub-grid scale physics. These new parameterizations include energetically constrained surface boundary layer dynamics (Reichl and Hallberg, 2018), mesoscale thickness mixing (Jansen et al., 2015), sub-mesoscale mixed layer re-stratification (Fox-Kemper et al., 2011), and shear-driven turbulence mixing in the interior ocean (Jackson et al., 2008). MOM6 is coupled with a dynamic and thermodynamic sea-ice model Sea Ice Simulator 2 (SIS2) (Adcroft et al., 2019). Currently, open lateral boundary conditions for sea ice are not implemented in MOM6-NEP.

As described in Drenkard et al. (2024), the horizontal grid of MOM6-NEP is based on an Arakawa C grid (Arakawa and Lamb, 1977), and has a resolution of ~1/10° (~ 9.7 km ± 0.5 km) with 342 × 816 tracer points. Horizontally, the model is an orthogonal curvilinear grid and extends from 10.8°N to 80.7°N and 156.6°E to 105.0°W (Fig. 1). In the vertical, a 75 layer z∗ remap coordinate (Adcroft and Campin, 2004) is used. The layer thickness is 2 m near the surface, gradually increasing to 250 m at

https://doi.org/10.5194/egusphere-2025-1229
Preprint. Discussion started: 13 May 2025

the deepest model depth of 6500 m. The shallowest bathymetry in the model is 5 m (i.e., areas where the true bathymetry is less than 5 m deep are set to 5 m). The domain has four open boundaries, the longest of which arcs through the Pacific Ocean and is here referred to as the "western" boundary.

MOM6-NEP is integrated forward in time with a split explicit method (Hallberg, 1997; Hallberg and Adcroft, 2009). It uses a variable barotropic timestep set to maintain stability, a baroclinic time step of 600 seconds, and a thermodynamic time step of 1200 seconds to increase computational efficiency (e.g., (Ross et al., 2023; Drenkard et al., 2024). Oceanic and atmospheric data sets used to force MOM6-NEP in this study are described in the next subsection (2.2).

2.1 Model Forcings

Initial and ocean open boundary conditions are specified using the high resolution (1/12°) Global Ocean Physics Reanalysis (GLORYS12v1; (Jean-Michel et al., 2021), which includes daily averages of 3-D ocean temperature, salinity, sea-surface height (SSH), meridional (v) and zonal (u) velocity components. GLORYS12 is one of the better-performing ocean reanalyses in coastal areas (Castillo-Trujillo et al., 2023; Amaya et al., 2023). Tidal forcing was obtained from the TPXO9 v1 model (Egbert et al., 2002). Ten tidal constituents are specified at the boundaries as was done in Ross et al. (2023) and Drenkard et al. (2024), including four semidiurnal constituents (M2, S2, N2, and K2), four diurnal constituents (K1, O1, P1, and Q1), and two long-period constituents (Mm and Mf).

The barotropic flow at the open boundaries is treated with a Flather boundary condition (Flather, 1976), and the baroclinic component is specified using the Orlanski boundary condition (Orlanski, 1976). The boundary flows are nudged to exterior velocities at timescales of 3 days for inflow and 360 days for outflow (Marchesiello et al., 2001). Nudging layers for temperature, salinity and velocities are applied to minimize noise at the boundaries that may contaminate the interior. River discharge is obtained from the Global Flood Awareness System version 3.1 (GloFAS, Zsoter, 2021).

In our study we used the 3-hour Japanese 55-year Reanalysis (JRA55) (Kobayashi et al., 2015) for atmospheric forcing, whereas Drenkard et al. (2024) used 1-hour ECMWF reanalysis v5 (ERA5) for this purpose. The JRA55 forcing variables include downward shortwave and longwave radiative fluxes, precipitation (separated into rain and snow), zonal and meridional winds, sea level pressure, air temperature and specific humidity. We used the JRA55-do version 1.5 (Tsujino et al., 2018), which is specifically tailored for driving ocean/sea-ice models. The bulk formulae of Large and Yeager (2004) were used to calculate surface buoyancy and momentum fluxes. Light attenuation within the water column is calculated following the Manizza et al. (2005) opacity scheme, which is influenced by monthly climatology of surface chlorophyll-a (Chl-a) concentration from the SeaWiFS satellite mission (NASA Ocean Biology Processing Group, 2018). Table 1 provides a summary of MOM6-NEP configuration, parameterization schemes, and parameter values used in this study, and relevant references.

https://doi.org/10.5194/egusphere-2025-1229
Preprint. Discussion started: 13 May 2025

Table 1: Base model configuration, parameterization schemes and associated parameter values, and relevant references.

Parameters	Value	Reference
Grid		
Horizontal	1/10°	
Vertical	75 layer z^*	Adcroft et al. (2019)
Time-stepping		
Baroclinic time step	600 s	
Thermodynamics time step	1200 s	
Planetary boundary layer parameterization	ePBL	Reichl and Hallberg (2018)
Mixed Layer re-stratification		
Sub-mesoscale eddy front length scale	800 m	Fox-Kemper et al. (2011)
Decay time scale	2.592×10^6 s	
Biharmonic viscosity	Maximum of Smagorinsky and resolution-dependent viscosities	
Smagorinsky coefficient	0.015	
Resolution-dependent	0.01 Δ_x^3 m^4 s^{-1}	Adcroft et al. (2019)
Bottom boundary layer mixing efficiency	0.0	
Background kinematic viscosity	0.0	
Background diapycnal diffusivity	8.0×10^{-6} m^2 s^{-1}	
Open Boundary Conditions		
Sea level and barotropic velocity	Flather scheme	Flather (1976)
Baroclinic velocity	Radiation and nudging scheme (3 day inflow, 360 day outflow timescales)	Marchesiello et al. (2001); Orlanski (1976)
Tracers	Reservoir length scales: 9000 m (out), 9000 m (in)	
Tides		
Explicit from TPXO9	10 tidal constituents: M2, S2, N2, K2, K1, O1, P1, Q1, MM, MF	Egbert and Erofeeva (2002)
Tidal SAL coefficient	0.01	Irazoqui Apecechea et al. (2017); Stepanov and Hughes (2004)
Opacity scheme	3-band with chlorophyll	Manizza (2005)

https://doi.org/10.5194/egusphere-2025-1229
Preprint. Discussion started: 13 May 2025

2.3 Evaluation datasets

The Optimum Interpolation Sea Surface Temperature (OISST) dataset (Huang et al., 2021) with spatial resolution of 0.25° × 0.25° is used to validate modeled sea surface temperature (SST). For sea surface salinity (SSS) evaluations, we used the northern North Pacific regional climatology version 2 (NNP RC; (Seidov, 2023) with a spatial resolution of 0.1° × 0.1° from the NOAA National Centers for Environmental Information (NCEI). NNP RC version 2 covers a period of seven decades. MOM6-NEP SSH is compared to absolute dynamic topography (spatial resolution of 0.25° × 0.25°) obtained from the Copernicus Marine Service's (Global Ocean Gridded L4) satellite altimetry dataset (Mercator Ocean, 2021).

During integration, MOM6-NEP computes the mixed layer depth (MLD) using instantaneous vertical profiles. The MLD is defined as the depth at which modeled potential density increases by 0.03 kg m^{-3} relative to its surface value. The computed MLD are then saved as daily averages. These are compared to the long-term MLD monthly climatology (1° × 1° spatial resolution) derived from profiles in the World Ocean Database and Argo datasets (De Boyer Montégut, 2024; De Boyer Montégut et al., 2004). The MLD in this dataset is also defined as the depth at which the density is 0.03 kg m^{-3} greater than the density of the surface layer, although its surface layer is at 10 m whereas the surface layer in MOM6-NEP is at 2 m. Daily sea-ice concentration data were retrieved from National Snow and Ice Data Center (https://nsidc.org/data/nsidc-0079/versions/4 and https://nsidc.org/data/nsidc-0081/versions/2). In addition to MLD, we also calculated thermocline depth, which is where the maximum vertical temperature gradient above a threshold of 0.1 °C/m occurs. When this threshold is not reached, the thermocline depth is assumed to be the water depth (70 m). This calculation is done using daily model output and temperature measured at M2.

Simulated daily bottom temperature on the Bering Sea shelf was sampled each year following the Alaska Fisheries Science Center (AFSC) Groundfish Bottom Trawl Survey; the “survey replicate” model output is then compared with bottom trawl data. Details on the bottom trawl data collection and postprocessing are described in Buckley et al. (2009) and Lauth (2011), and the data are available at https://github.com/afsc-gap-products/coldpool. The cold pool spatial distribution and its interannual variability were constructed following the method described in Kearney (2021), and the same method is applied to both modeled and survey data.

2.4 Moorings

Modeled temperature and salinity are evaluated against the long-term Bering Sea biophysical mooring data along the 70-m isobath (Fig. 1; Stabeno et al., 2023). Moorings at M2 (56.87°N, 164.06°W) are deployed and recovered twice a year, once during the spring (April/May) and again in late summer or early autumn (September/October). The September/October

https://doi.org/10.5194/egusphere-2025-1229
Preprint. Discussion started: 13 May 2025

deployment is a subsurface mooring with the uppermost instrument at 11 m. The spring deployment is a surface mooring. Moorings at M2 have been maintained since 1995 (Stabeno et al., 2010; Stabeno et al., 2023), although there are some gaps primarily due to fishing. Mooring M4 (57.9 °N, 168.9 °W) has been maintained since 1998, while the last two mooring sites, M5 (59.9 °N, 171.7 °W) and M8 (62.2 °N, 174.7 °W), have been maintained since 2005. M4 is typically turned around (recovered and redeployed) in the spring, while M5 and M8 are turned around in the late summer. The primary moorings are built using chain to safeguard against potential damage from sea ice and the significant fishing activity in this region. The moorings were equipped with instruments that collect a wide variety of data: temperature (miniature temperature recorders, SBE-16, SBE-37 and SBE-39), salinity (SBE-16, SBE-37), nitrate, and chlorophyll fluorescence (WET Labs DLSB ECO Fluorometer). A companion mooring at each site measures currents using a 300-kHz acoustic Doppler current profiler (ADCP).

Since 2018, the summer mooring at M2 has contained a Prawler (Profiling crawler; used in 2018), that measures temperature, salinity, fluorescence, O2, and pressure in the upper ~45 m (Stabeno et al., 2023; Stalin et al., 2023). Prior to 2018 and during the winter at M2, the vertical sampling resolution in the upper 30 m is ~3 m, and in the bottom 40 m is ~ 5 m. The winter mooring remains deployed for one year. A similar resolution occurs at M4 (upper instrument at 11 m), M5 (upper instrument at 15 m) and at M8 (upper instrument at 20 m). All instruments sample at least hourly and are calibrated prior to deployment. All data are processed in accordance with the specifications provided by the manufacturers.

A summary of observational datasets, their resolution, and sources used to evaluate MOM6-NEP is shown in Table 2. To compare model output against different data products, we used the xesmf Python Package (Zhuang et al., 2023) to bi-linearly interpolate the dataset with higher resolution onto the horizontal grid of the product with lower resolution.

Table 2: Summary datasets used for evaluation of MOM6-NEP model performance.

Dataset	Variable	Resolutions	Reference
OISST v2	Sea surface temperature	0.25° × 0.25° Time: daily, monthly	Huang et al. (2021)
NNP Regional Climatology (NNP RC v2)	Sea surface salinity	0.1° × 0.1°	Seidov et al., (2023)
Global Ocean Gridded L4 (Satellite altimetry)	Sea surface height	0.25° × 0.25°	Mercator Ocean (2021)
deBoyer MLD Climatology	Mixed layer depth	1° × 1°	de Boyer Montégut (2023)
Eco-FOCI Moorings	Temperature Salinity	Time: hourly	Stabeno et al., (2010, 2023)

https://doi.org/10.5194/egusphere-2025-1229
Preprint. Discussion started: 13 May 2025

AFSC Groundfish Bottom Trawl Survey	Bottom temperature	---	Buckley et al., 2009; Lauth et al., 2011
NASA NSIDC	Sea-ice concentration	0.25° × 0.25° Time: daily	NSIDC

205

3 Results

3.1 Refinement of the shear-driven vertical mixing

The default Jackson et al. (2008) parameterization of shear-driven turbulence was found to over-mix the Bering Sea shelf, eroding the thermocline in summer; this was especially true in the southern domain which is characterized by strong tides. To account for the additional turbulent processes that disrupt the growth of shear-driven turbulence which is not captured by the default Jackson scheme, we introduced a rescaling factor, *lz_rescale* (β) to the formulae of decay length scale (L_d) for eddy diffusivity (κ) such that

$$L_d = min(\lambda L_b, \beta L_z)$$

where λ is a non-dimensional scaling factor, L_b is the buoyancy length scale, and L_z is the distance to the nearest vertical boundary.

In the original formulation, β is effectively one, resulting in the unmodified contribution of L_z to L_d.

We tested different values of λ and β, along with perturbations to several other model parameters (C_N, C_S, and Ri_c) in a suite of sensitivity tests. C_N and C_S are non-dimensional turbulent kinetic energy dissipation coefficients associated with stratification and shear, respectively, while Ri_c is the critical Richardson number. Our perturbed values of these parameters are within the bounds of theoretical arguments (Jackson et al., 2008). We also turned off tidal forcing in one sensitivity test. The vertical profiles of shear-driven diapycnal diffusivity from the sensitivity tests and the control simulation (*CTRL*) are shown in Fig. 3. *CTRL* exhibits strong shear-driven vertical diffusivity in the bottom boundary layer with a local maximum around 50-m, and its magnitude is approximately 7-8 times bigger than shear-driven mixing in the surface boundary layer. With this strong mixing, the modeled water column at M4 is well mixed even in summer, missing the well-defined thermocline in observations. Such strong mixing has significant implications for nutrient dynamics and biological processes. The "No-Tides" run suggests that this over-mixing is strongly coupled to tidal dynamics in the bottom boundary layer. Increasing Ri_c promotes even more mixing, consistent with dynamical understanding of the critical Richardson number. Increasing dissipation through larger C_N and C_S (than in *CTRL*) results in a limited decrease in mixing. Changing both λ and β (green dotted and purple dashed lines, Fig 3) achieves similar effects to perturbing β alone (red and olive solid lines, Fig. 3).

https://doi.org/10.5194/egusphere-2025-1229
Preprint. Discussion started: 13 May 2025

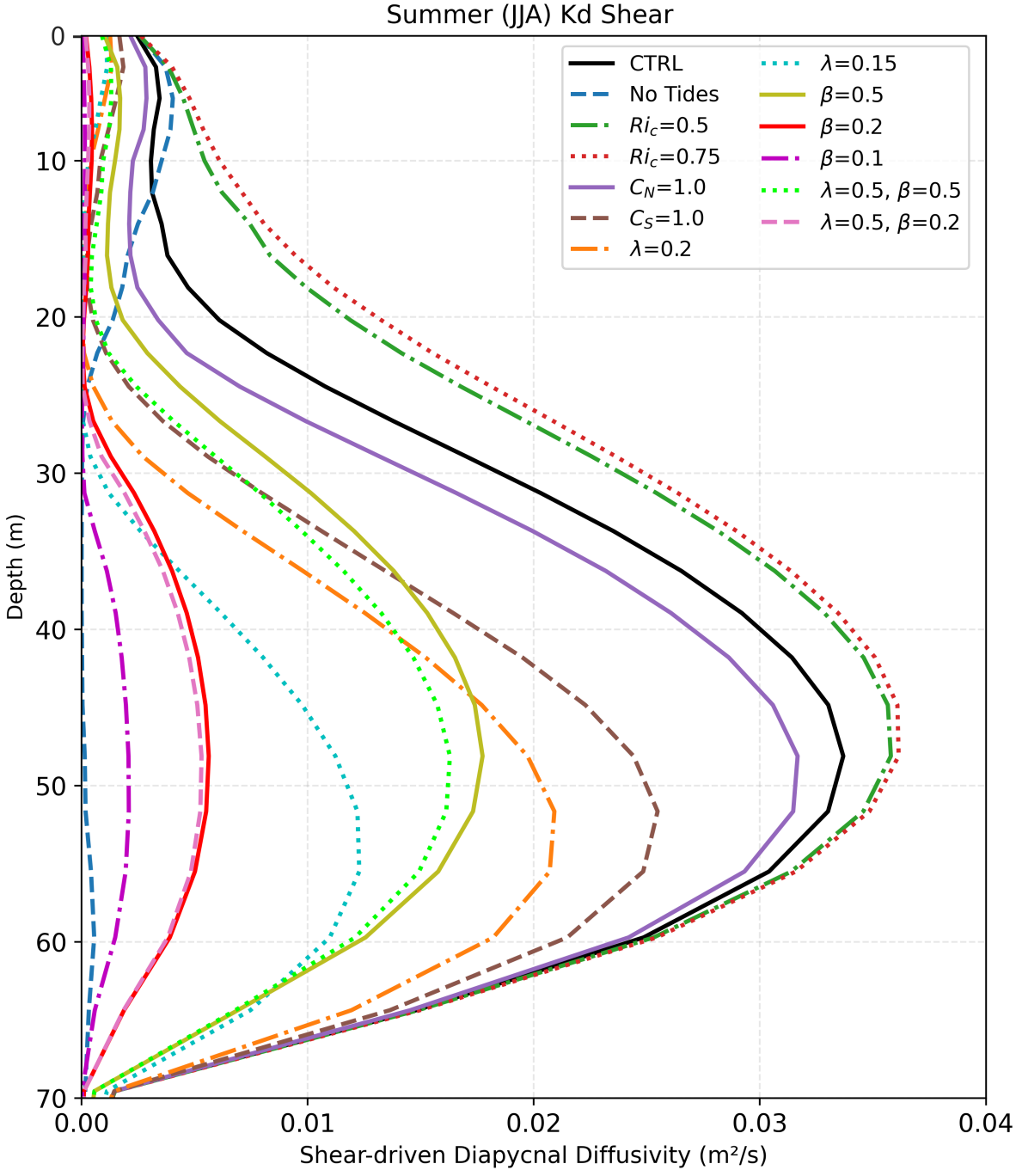

Figure 3: Vertical profiles of shear-driven vertical mixing coefficient in the summer (June-July-August average) of 2000 at the M4 location from the control simulation (CTRL, black solid line) and the sensitivity tests (colored lines). In each of the sensitivity tests, only the parameters specified in the line legend are perturbed, while all other parameters remain unchanged from CTRL.

https://doi.org/10.5194/egusphere-2025-1229
Preprint. Discussion started: 13 May 2025

The effects of these perturbations on the modeled summer bottom temperatures at the mooring locations and their comparisons with observations are summarized by a Taylor diagram (Fig. 4). Across all mooring locations, experiment β=0.2 (represented by the red square) consistently maintains its proximity to the OBS point (Fig. 4a-d), showing low RMSE relative to OBS, nearly perfect reproduction of the observed interannual variability, and strong correlation with OBS (R > 0.92). In contrast, *CTRL* (black star) and experiments Ri_c = 0.5 and Ri_c = 0.75 (green and red hexagon, respectively) show significant deviations from *OBS*. Other sensitivity tests (with the exception of the "No Tides" experiment) generally fall between the *CTRL* and β=0.2. The "No-Tides" experiment shows much weaker interannual variability of bottom temperature than *OBS* and other sensitivity experiments, highlighting the importance of tides, tidally induced mixing and its interactions with other oceanic processes.

https://doi.org/10.5194/egusphere-2025-1229
Preprint. Discussion started: 13 May 2025

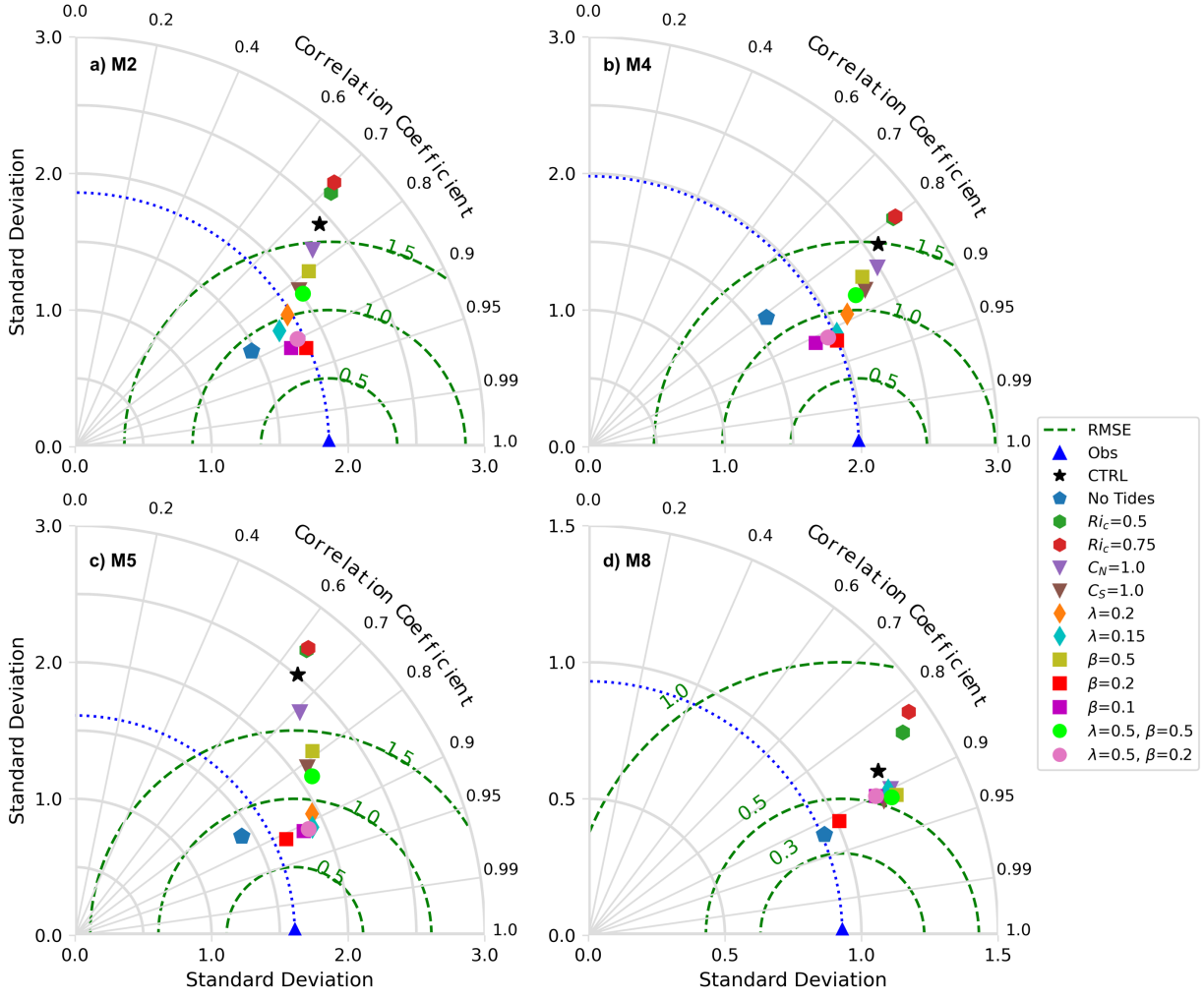

Figure 4: Taylor diagram showing the standard deviation of both modeled and observed bottom temperature, along with correlation coefficients and root mean squared errors (RMSEs) between the modeled and observed bottom temperature at the mooring locations (a) M2, (b) M4, (c) M5, and (d) M8. Results from OBS, CTRL, and sensitivity tests are represented by distinct symbols, with the symbol legend displayed on the right. Note that the x- and y-axis scales in panel (d) are half of those in the other panels. These statistics were calculated using the monthly means of bottom temperature from the respective mooring periods (M2: 1995-2018, M4: 2000-2018, M5: 2005-2018, M8: 2005-2018).

In addition to the point-wise comparison, we also examined the modeled shelf-wide bottom temperature against the AFSC bottom trawl survey. In this evaluation, daily temperatures from the model are first subsampled in time and horizontal locations following the survey data, generating survey-replications of the model output. Fig. 5 shows scattered plots between survey and survey-replicated model output from *CTRL* and the best fit experiment β=0.2 (Fig. 4) over the hindcast period (1993-2018).

https://doi.org/10.5194/egusphere-2025-1229
Preprint. Discussion started: 13 May 2025

Experiment β=0.2 shows a tighter correspondence with observations than CTRL, having reduced bias (0.42 to 0.24 °C) and RMSE (1.33 to 0.97 °C), and higher correlation coefficient (0.82 to 0.90). These results indicate that limiting shear-driven vertical mixing through *lz_rescale* improves the model's capacity to replicate bottom temperature dynamics, particularly under Bering Sea tides (~ 30 cm s^{-1}). Interestingly, observed temperatures in the warmest range (>13°C) that occurred primarily in 2016-2018 (yellow) tend to be cooler than the modeled temperatures in the same years. This will be further explored in section 3.4.

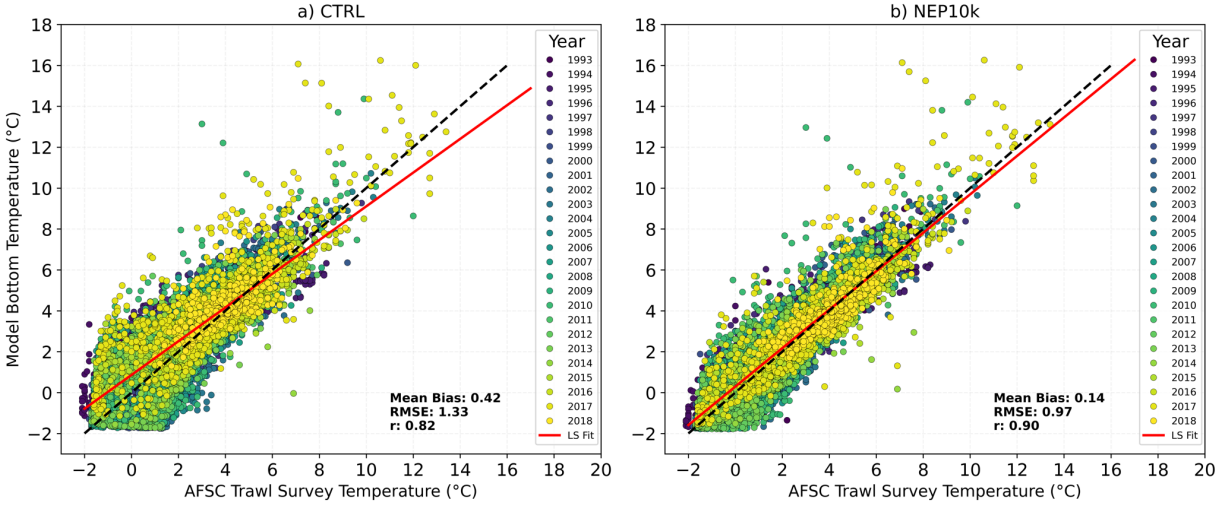

Figure 5: Scatter plots of temperature from the AFSC bottom trawl survey (x-axis) versus modeled survey-replicated bottom temperature (y-axis) from (a) CTRL and (b) the β=0.2 experiment. Data point colors represent different years. The red lines represent the least square fits, while the black dashed lines indicate the 1:1 relationship.

Since experiment β=0.2 provides the overall best fit with observations, this parameterization is used in all ensuing analyses. We refer to this particular model configuration as MOM6-NEP10k v1.1P, where P stands for "physics only". The main differences between MOM6-NEP10k v1.1P and MOM6-COBALT-NEP10k v1.0 (Drenkard et al., 2024) are: (1) MOM6-COBALT-NEP10k v1.0 is coupled to marine biogeochemical processes (the internally generated phytoplankton influence shortwave absorption) whereas MOM6-NEP10k v1.1P is physics only (a satellite-derived phytoplankton climatology is imposed); (2) atmospheric forcing in MOM6-NEP10k v1.1P is JRA55 while in MOM6-COBALT-NEP10k v1.0 it is ERA5; (3) MOM6-COBALT-NEP10k v1.0 uses the Bodner scheme (Bodner et al., 2023) where mixed layer submesoscale frontal length is calculated dynamically whereas in MOM6-NEP10k v1.1P it is specified as a constant (800 m).

https://doi.org/10.5194/egusphere-2025-1229
Preprint. Discussion started: 13 May 2025

3.2 Circulation

MOM6-NEP10k v1.1P replicates the main current systems in the northern Gulf of Alaska and Bering Sea (Fig. 2a). In the Gulf of Alaska, the Alaskan Stream - the southwestward flowing western boundary current of the eastern Subarctic Gyre (Stabeno and Hristova, 2014) is clearly evident (Fig. 2b). Over half of this transport flows through the deeper passes (e.g., Amukta Pass, Amchitka Pass, and Near Strait) to form the Bering Sea Gyre (Stabeno et al., 2005; Stabeno, 1999; Reed and Stabeno, 1993). Each branch of the Bering Sea Gyre (Aleutian North Slope Current (Stabeno et al., 2009; Reed and Stabeno, 1999), the Bering Slope Current (Ladd, 2014), and the Kamchatka Current (Stabeno et al., 1994)) is well-represented in the model simulations (Fig. 2a, b).

The flow on the broad, eastern shelf is generally northward (Fig. 2a). Once again, the model replicates the current systems (Fig. 2b). There are two well defined currents on the eastern shelf (Stabeno et al., 2016): the Alaska Coastal Current (ACC) which flows northward along the 50-m isobath (the boundary between coastal domain and middle shelf domain) and northward flow along the 100-m isobath. The ACC eventually flows through the eastern side of Bering Strait. The flow along 100-m isobath joins with the Anadyr Current which flows eastward along the southern side of the Siberian coast and enters the Arctic through the western side of Bering Strait.

The magnitude of flow through the Aleutian Passes is critical for the transport of heat and salts northward into the Bering Sea. In addition, the only source of Pacific water into the Arctic is through the Bering Strait. A careful comparison of the magnitude of transport through the passes is beyond the scope of this paper and will be explored in a later manuscript.

3.3 Sea-ice extent and seasonal timing

Sea ice structures the Bering Sea shelf, from ocean temperature to timing of the spring bloom to the range of fish species. While the eastern Bering Sea (here defined as the region north of Aleutian Islands, south of 66°N, and east of 178°E) is ice free in the summer, maximum areal ice extent in winter varies among years, ranging from $< 0.4 \times 10^6$ km^2 in warm years to 1.0×10^6 km in cold years (Fig. 6b). In the satellite-era, the largest ice extent occurred in 2012 when it covered almost the entire eastern shelf, while the smallest extent occurred in 2018, when ice was largely confined to the northern shelf (Fig. 6a, purple and blue lines). This warm-to-cold year contrast is well captured by the model (Fig. 6). The long-term (1993-2018) mean ± standard deviation of areal ice extent in March (the month with maximum ice) is 0.65 ± 0.14 x 10^6 km^2 in MOM6-NEP, compared to $0.71 \pm 0.14 \times 10^6$ km^2 in satellite data.

https://doi.org/10.5194/egusphere-2025-1229
Preprint. Discussion started: 13 May 2025

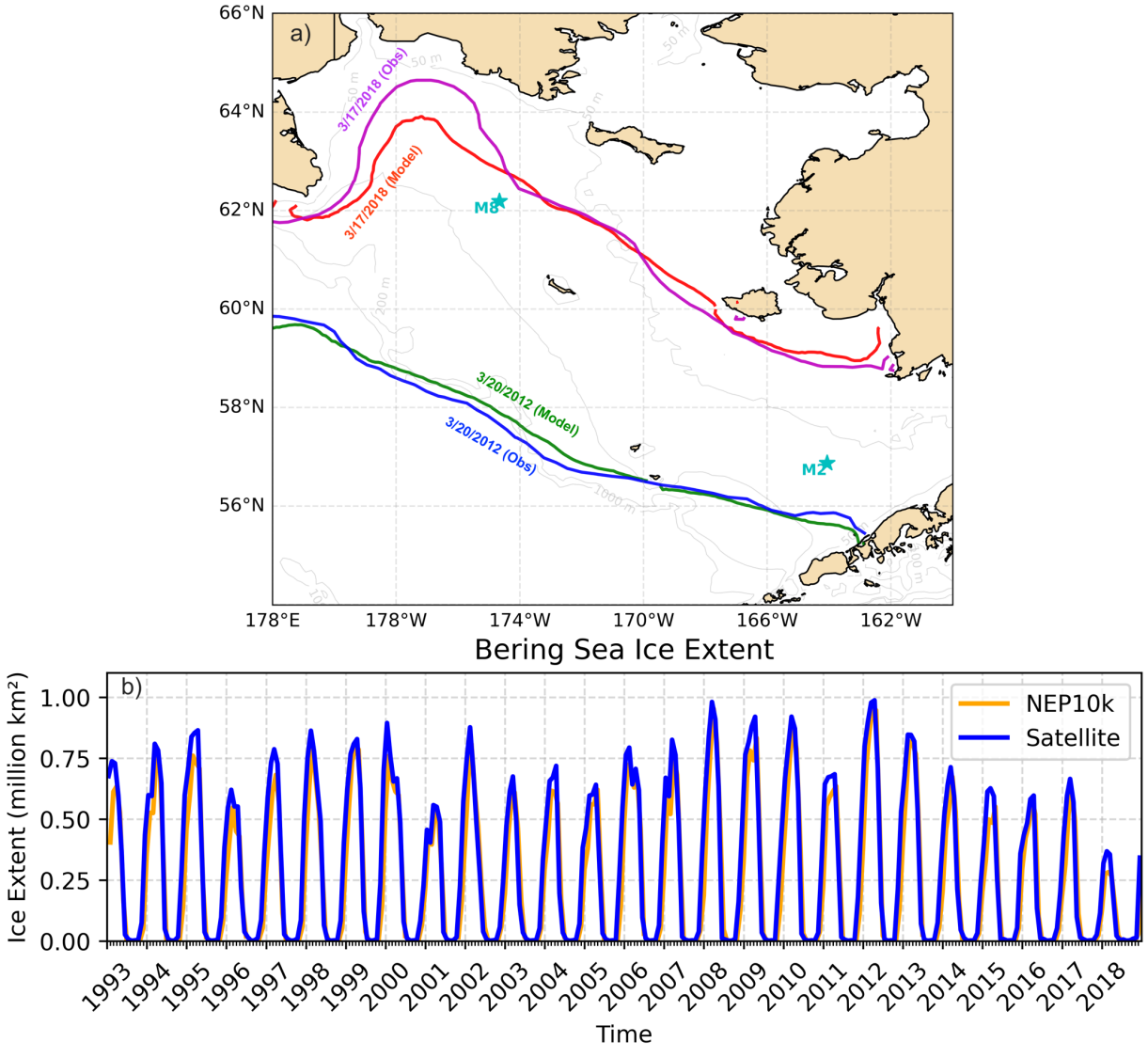

315

Figure 6: (a) Ice edge defined by the 10% ice concentration in two extreme years, 2012 and 2018. (b) Monthly mean areal sea-ice extent over the Bering Sea from MOM6-NEP10K (orange line) and satellite observations (blue line). Ice extent is defined as the total area of grid points with ≥ 10% ice cover. The satellite data was obtained from the National Snow and Ice Data Center, using the "climate data record" monthly ice concentration at 25 km × 25 km horizontal resolution.

320

Sea-ice cover at the mooring locations is further evaluated against satellite observations. At M2, there is large interannual variability in sea ice. Since 2000 there have been a series of cold years with extensive sea ice (e.g., 2007-2013), and warm years with little/no ice reaching the southern shelf (2001-2005 and 2014-2022) (Stabeno et al., 2023). At M8, sea ice is far

https://doi.org/10.5194/egusphere-2025-1229
Preprint. Discussion started: 13 May 2025

more persistent, but even here there are years with more persistent sea ice (e.g., 2006-2013, excluding 2011). MOM6-NEP not only replicates the areal ice coverage in the entire Bering Sea (Fig. 6), but also reproduces both seasonal and interannual variability at M2 and M8 (Fig. 7).

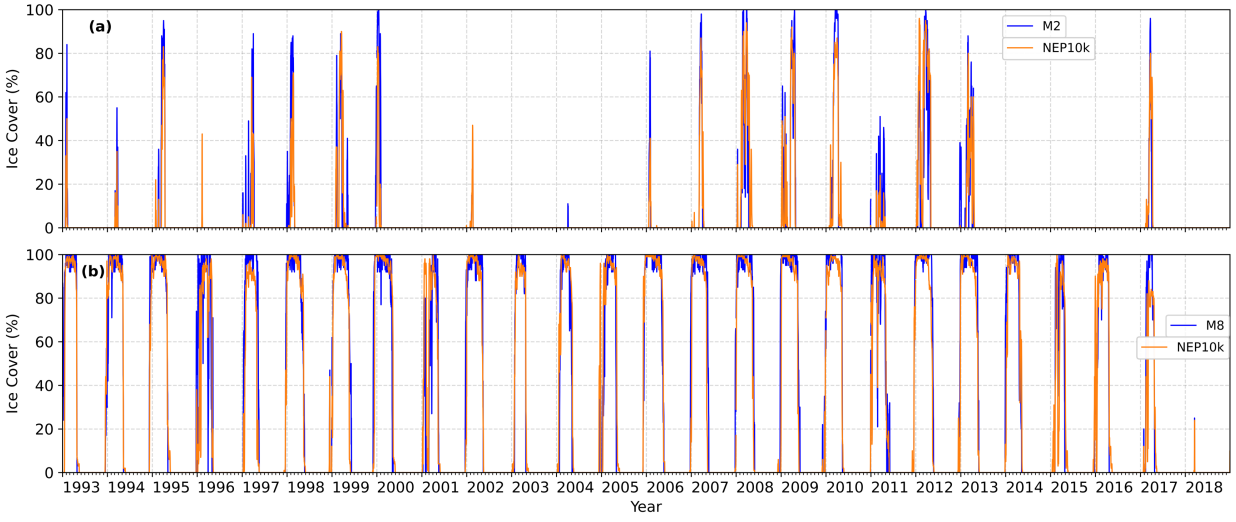

Figure 7: The averaged ice cover (percentage) in a 25 km × 25 km box centered on the mooring sites from MOM6-NEP10K (orange line) and satellite observation (blue line) at (a) M2 and (b) M8.

A more detailed examination of the difference between modeled and observed daily ice concentration at the mooring sites (Fig. 8) reveals striking patterns. First, the mean seasonal signal from observations is replicated by the model at both M2 (Fig. 8b) and M8 (Fig. 8d), where the timing of modeled ice arrival and retreat closely matches the observed timings, although the model tends to underestimate sea-ice cover at these locations by a small amount at the beginning and at the end of the ice season. This agreement in the timing of seasonal ice advance and retreat is a notable improvement from previous studies using global or regional models (e.g., Cheng et al., 2014; Kearney et al., 2020).

https://doi.org/10.5194/egusphere-2025-1229
Preprint. Discussion started: 13 May 2025

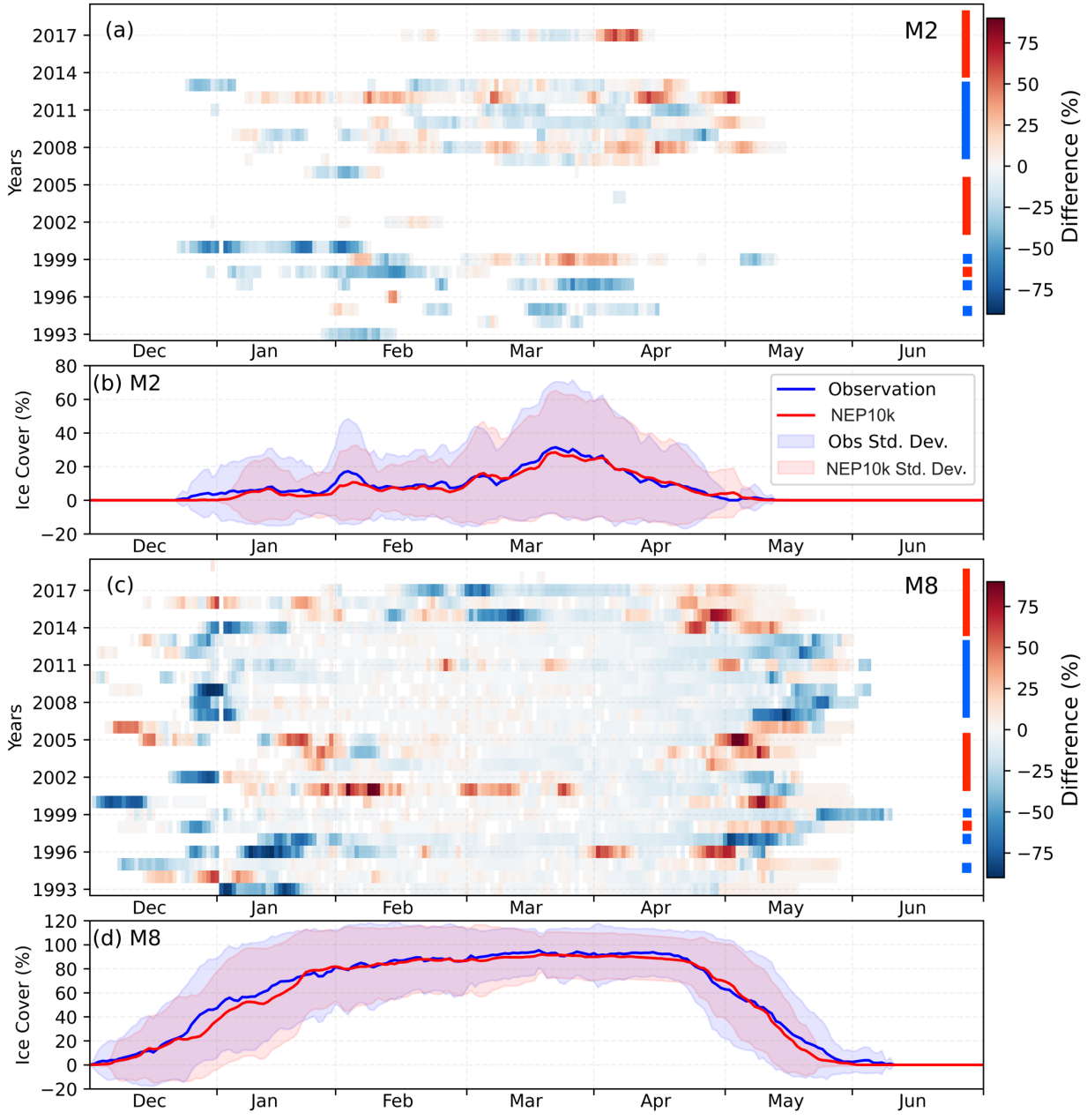

Figure 8: Discrepancies between modeled and observed daily ice concentration (modeled minus observation) at mooring locations (a) M2 and (c) M8. Climatology (averaged over 1993-2018) of observed (blue line) and modeled (red line) daily ice concentration at (b) M2 and (d) M8; shading represents one standard deviation of the interannual variability. Blue and red vertical bars on (a, c) correspond to anomalously cold and warm periods, respectively.

https://doi.org/10.5194/egusphere-2025-1229
Preprint. Discussion started: 13 May 2025

At both mooring sites, the greatest discrepancies are during ice formation (December-early January) and ice melt (typically April at M2 and May at M8) (Fig. 8a, c). The discrepancy at M2 is smaller than at M8. This is particularly true during 2001-2005, 2014-2016 and 2018. This is not surprising, since sea ice did not penetrate into the southern shelf during these years, and this lack of ice was replicated in the model output (Fig. 8a). At M8 discrepancies occurred throughout the study period, except 2018 when there was no ice at M8 (Stabeno and Bell, 2019). One pattern that persists is that in years with more ice (e.g., 1999, 2007-2013), the simulation tends to have earlier than observed ice retreat (represented by the negative discrepancies), whereas in years with less ice (e.g., 2001-2005, 2014-2018), the M8 simulations tend to have later than observed ice retreat (represented by the positive discrepancies).

One possible explanation for this pattern is that the model melts all ice at the same rate. Thus, it melts thicker, older ice at the same rate as younger, thinner ice; however, studies (e.g., Hunke, 2014) found that older ice melts more slowly than younger ice. Thus, the model appears to melt young ice too slowly and old ice too fast, resulting in the noted discrepancy. M2 does not show this systematic bias pattern because it is mostly young ice. In addition, ice on the southern shelf can be influenced by wind forced advection (retreat) in addition to just local melting (Stabeno et al., 2012).

3.4 Sea surface temperature and salinity, mixed layer depth, and sea surface height

Both the modeled and OISST mean SST (Fig. 9a, b) show strong gradients oriented roughly parallel to the shelf break. Overall, simulations were cooler on the shelf, but warmer in the deeper basin (Fig. 9c). The largest cold biases were in the Chukchi Sea, and were primarily caused by biases in the summer months (Fig. 10c). Why the agreement in the summer was poorer than the other seasons is unclear. One possible explanation is that SST in summer is highly sensitive to maximum ice extent and the timing of ice retreat the previous spring. Small errors in ice extent or timing of ice retreat, combined with strong solar radiation, can result in larger errors in the summer SST.

https://doi.org/10.5194/egusphere-2025-1229
Preprint. Discussion started: 13 May 2025

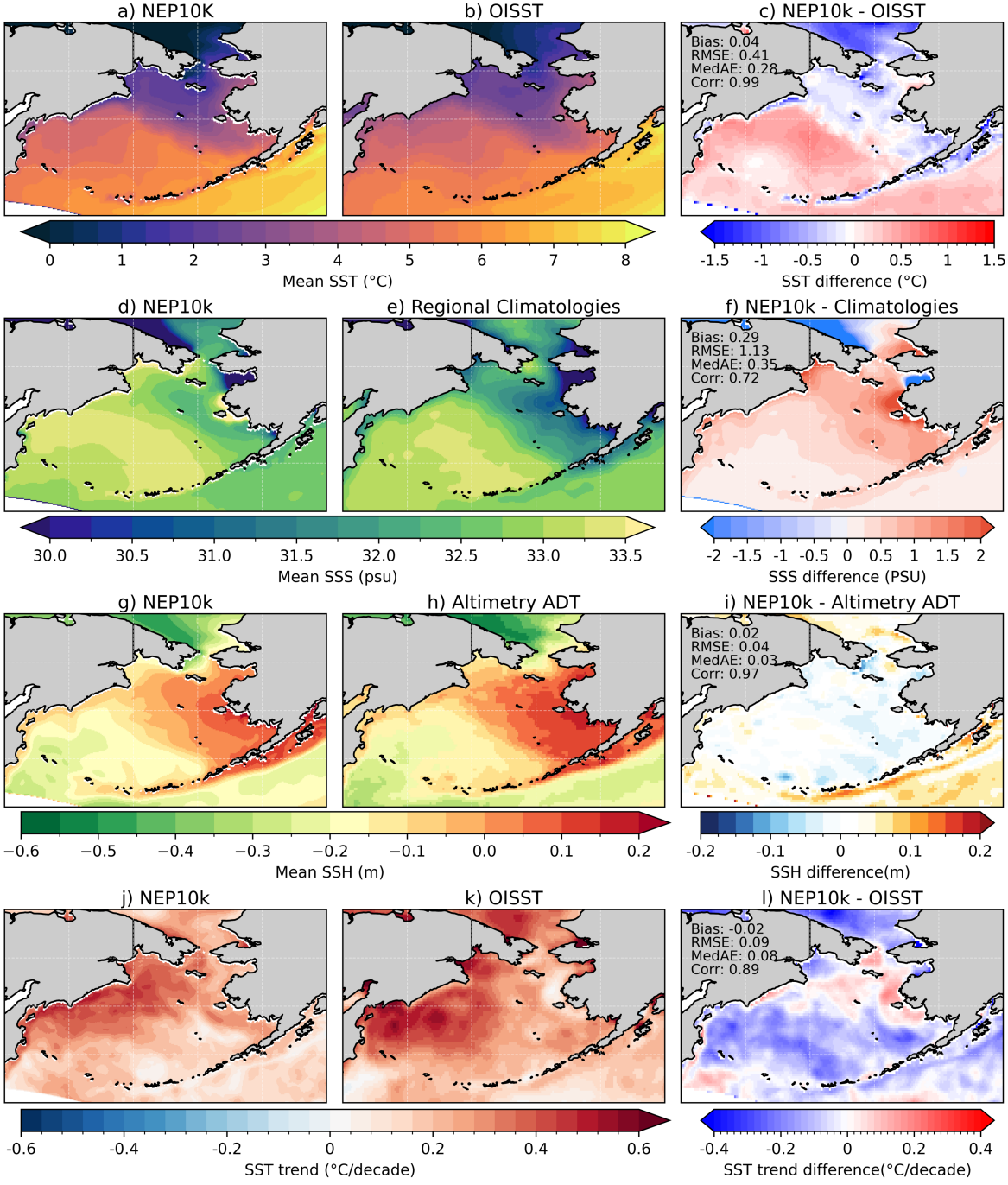

Figure 9: Mean SST (1993-2018) from (a) MOM6-NEP10K and (b) OISST, and (c) their differences. Mean SSS from (d) MOM6-NEP10K and (e) regional climatologies, and (f) their differences. Mean SSH from (g) MOM6-NEPK10K and (h) satellite altimetry, and (i) their differences. SST trends, defined by least-fit linear regression from (j) MOM6-NEP10K (k) OISST and (l) their differences. All correlation values are significant ($p<0.001$). Statistics of the biases (domain averaged mean bias, RMSE, MedAE, and correlation coefficient) are indicated on panel c), f), i), and l).

https://doi.org/10.5194/egusphere-2025-1229
Preprint. Discussion started: 13 May 2025

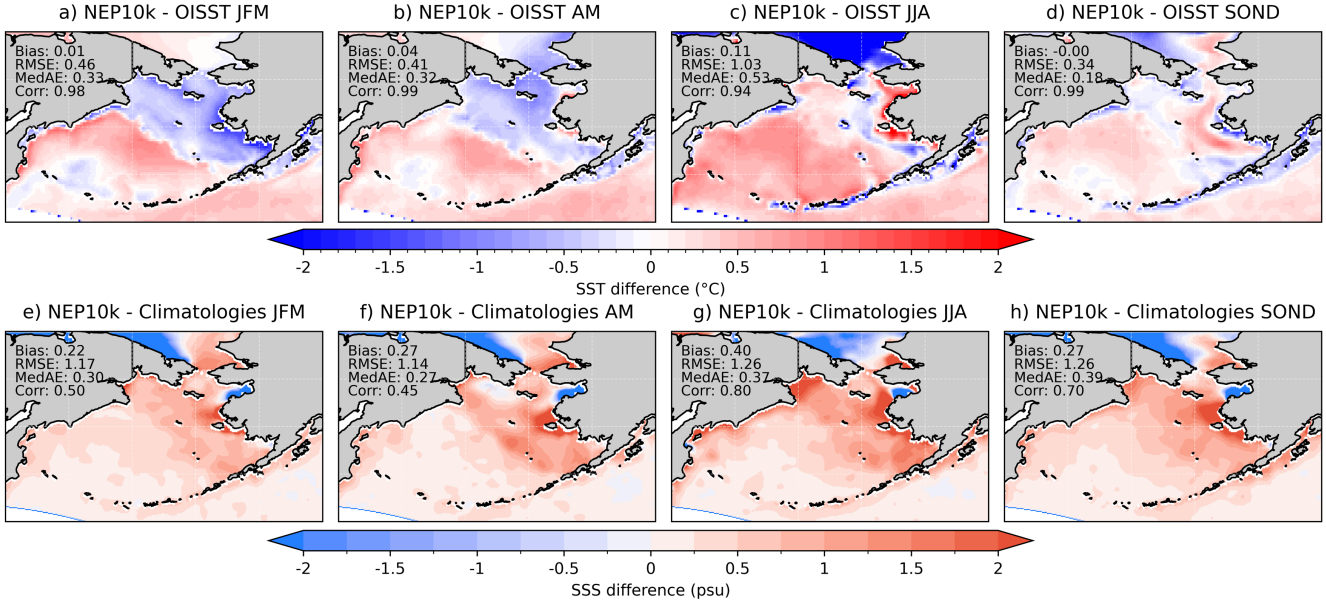

Figure 10: Difference between the 1993–2018 seasonal mean SST in the model and the OISST dataset for: (a) January-March, (b) April-May, (c) July-September, and (d) October-December. Similarly, the seasonal differences in SSS for: (e) JFM, (f) AM, (g) JAS, and (h) OND. Bias statistics are summarized in each panel.

Similar to SST, Fig. 9d-f compares mean SSS (1993-2018), simulated by model (Fig. 9d) against regional climatologies (Fig. 9e). Along the northern Siberian coast, the model is consistently fresher than the observations. This may be associated with sea-ice biases due to the closed ice boundary conditions and limited observational data. Modeled mean SSS patterns over the Bering Sea basin tend to be in good agreement with regional climatologies, with small (<0.5 psu) discrepancies (Fig. 9f); SSS biases on the Bering Sea shelf, however, are larger than those in the basin (Fig. 9f). The saltier SSS bias on the eastern shelf coincides with colder SST biases, leading to positive sea surface density biases in the region. The positive SSS bias along the eastern Bering Sea coast tends to be stronger in JJA (Fig. 10g) than in other seasons: the model shows small positive biases during JFM and AM (Fig. 10e, f), and moderately positive bias in SOND (Fig. 10h), mainly in the central and southern inner shelf.

Model and observations show a similar spatial pattern in SSH (Fig. 9 g-h): higher values in the central and southeastern Bering Sea shelf; decreasing SSH in the basin; and lower SSH along the north coast of Siberia in the Chukchi Sea. SSH bias over the entire Bering Sea is modest (Fig. 9i). Not unexpectedly, MOM6-NEP simulation and OISST reveal a warming trend (Fig. 9j, k). The spatial structure of SST warming is similar across the datasets, with stronger warming (> 0.3 °C/decade) along the Russian coast and in the Chukchi Sea, but weaker warming elsewhere. Nowhere is there cooling. Quantitatively, the model

https://doi.org/10.5194/egusphere-2025-1229
Preprint. Discussion started: 13 May 2025

simulation tends to overestimate the SST warming on the northern Bering Sea shelf and in the North Pacific adjacent to the western Aleutian Islands, but underestimate it in the rest of the domain (Fig. 9l).

There is reasonable agreement between the model and observed MLD during the summer except in the southern basin (Fig. 11c). The model on average underestimates the summer MLD, although there were both positive and negative spatial patterns in the biases. MLD biases in winter increase significantly relative to summer values. The modeled winter MLDs are too deep nearly everywhere across the domain. Interestingly, the spatial correlation remains high (Fig. 11f). MLD biases can be linked to errors in surface forcing, model physics, inaccuracies in numerical algorithms, and/or uncertainties in observations, but which factor is the main contributor is unknown. MLD and its seasonal evolution affect nutrient distribution and primary production, and is crucial to the marine ecosystem dynamics of the region. Further quantifying the modeled MLD and its spatiotemporal variability, and understanding the mechanisms contributing to its biases will be a research priority in the future.

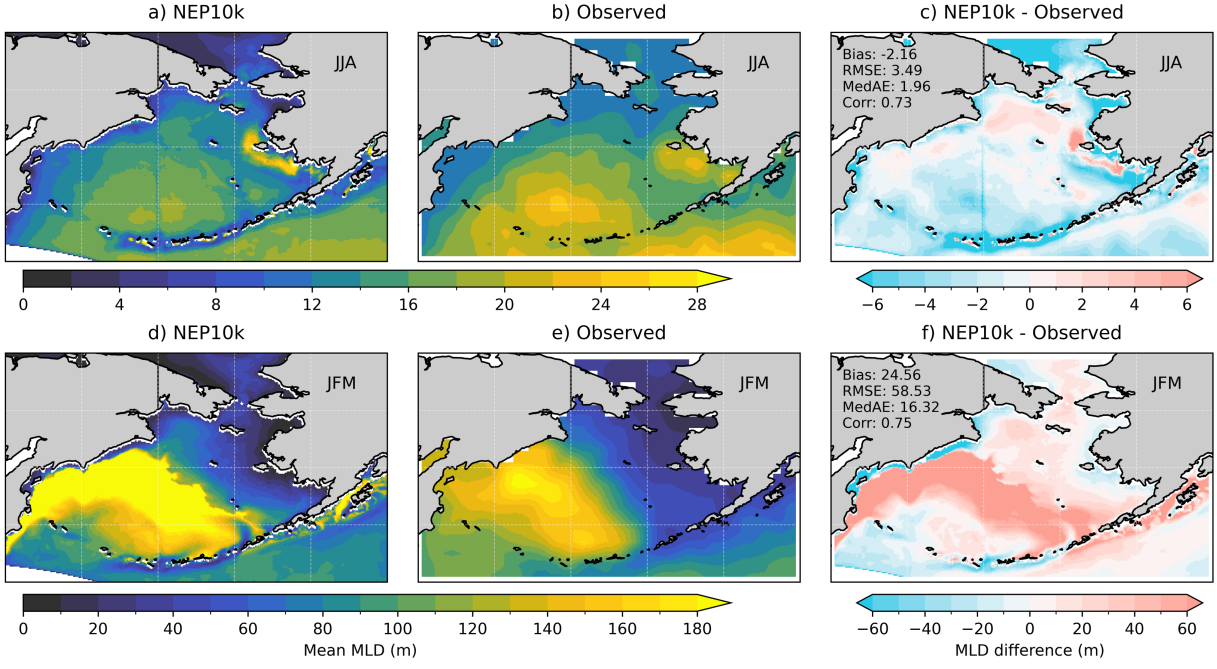

Figure 11: Mean (1993-2018) MLD from the model for (a) summer (June-August) and (d) winter (January-February). MLD from the observation-based climatology of de Boyer Montégut (2004) for (b) summer and (e) winter. The difference between modeled and observations for (c) summer and (f) winter, including bias statistics.

https://doi.org/10.5194/egusphere-2025-1229
Preprint. Discussion started: 13 May 2025

3.5 Water column structure: temperature and salinity

3.5.1 Southern Bering Sea (M2)

Figure 12a illustrates the depth-time contours of temperature collected at M2. The seasonal pattern is clearly evident - warm (>8°C) temperatures near the surface in the summer, cooling and mixing in the fall, and cold (usually <2°C) temperatures throughout the water column in winter and into spring. The surface wind mixed layer in summer was ~20 m deep and there is a tidally-mixed bottom layer. These seasonal patterns are accurately replicated by the model (Fig. 12b), as is the mean vertical structure during each season (Fig. S1a-d).

https://doi.org/10.5194/egusphere-2025-1229
Preprint. Discussion started: 13 May 2025

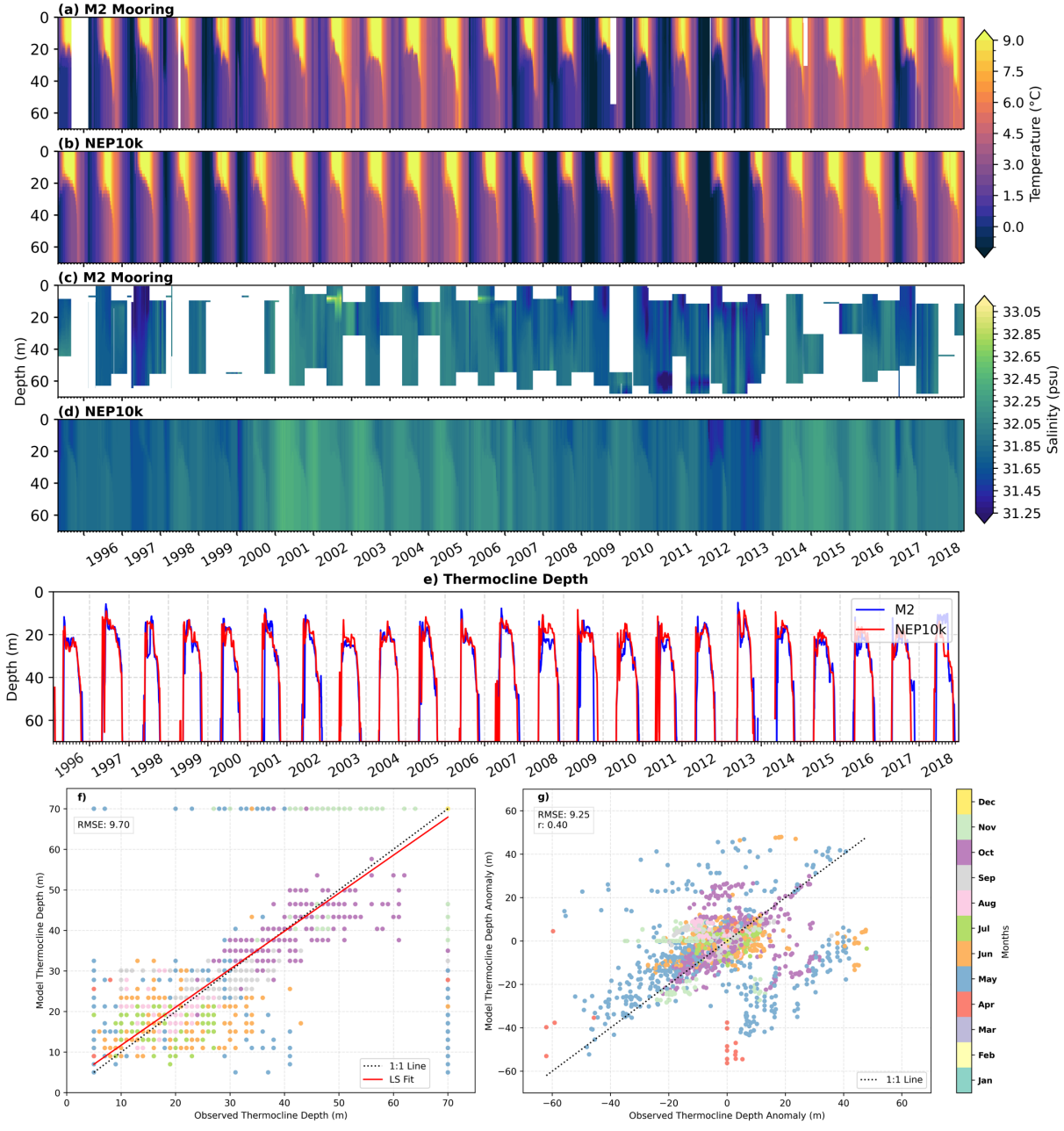

Figure 12: Depth versus time contours of temperature for (a) observations and (b) model, and salinity for (c) observations and (d) model. (e) The thermocline depth at M2 for model (red) and observations (blue). Scatter plots of: (f) observed versus modeled daily thermocline depth at M2; and (g) thermocline depth anomaly with the mean signal (1996-2018) removed.

https://doi.org/10.5194/egusphere-2025-1229
Preprint. Discussion started: 13 May 2025

Salinity data from the moorings are more limited, but interannual variability is evident (Fig. 12c). The water was relatively fresh in 1993-1999 and 2007-2013, and relatively salty in 2000-2005 and 2014-2018. The fresher (saltier) conditions tend to occur in colder (warmer) years, consistent with colder years having more sea ice at M2 that melts upon arrival, thus freshening the water column. This interannual variability is captured by the model (Fig. 12d), although the simulated salinity appears smoother, lacking some of the higher salinity peaks and short-term variability characteristic of the mooring data. This suggests that the model may underrepresent certain episodic salinity events, despite its ability to accurately simulate the mean salinity distribution.

The thermocline depth and strength are crucial for understanding marine ecosystems since they influence nutrient availability, primary productivity, and the distribution of marine species, thus influencing the bigger ecological and fisheries dynamics in the Bering Sea. Thus, we examine the thermocline in more detail. Here the thermocline depth is defined as the depth where the maximum vertical temperature gradient (threshold > 0.1 °C/m) occurs. The observed and modeled thermocline depth displays a clear seasonal cycle (Fig. 12e): it shoals in late spring and summer due to surface heating and reduced wind mixing, allowing the water column to stratify, and deepens in fall and winter due to surface cooling and mixing processes. The consistency between the observed and modeled thermocline depth suggests that the model captures the key physical process regulating seasonal stratification on the Bering Sea shelf. The relatively small discrepancies between the model and observations in certain years (e.g., 2008 in Fig. 12e) can be caused by inaccuracy in forcing functions (e.g., surface heating, winds) or subgrid scale parameterizations.

A more quantitative comparison between modeled and observed thermocline depth suggests that the water column is stratified mainly from May to October (Fig. 12f, colors of the dots) and is well mixed during the rest of the year (e.g., the points at (70, 70)). Wind-mixed deepening occurs during October (purple dots on Fig. 12f). There are generally no systematic biases between the model and observations as the data points are distributed above and below the 1:1 line. It is more common for the OBS to be well mixed than the model (pending plot revision; the 0.1 threshold business).

More patterns are revealed once the annual signal is removed (Fig. 12g). Most of the data is centered around (0,0); ~80% (~90%) of the data points are within 5 m (10 m) of the origin suggesting small biases. If we just consider the summer months when the water is stratified, the percentages are less (~68% with 5 m, and ~85% within 10 m).

The greatest persistent deviations from the 1:1 line occur in May when the system usually becomes stratified (Fig. 12g, blue dots), and around October when the thermocline deepens (Fig. 12g, purple dots). These results suggest that the rapidly changing transition seasons (spring and fall) still pose challenges for modeling accuracy, which has implications for seasonal forecasting of the ocean environment and marine ecosystem across these seasons (e.g., the so-called spring predictability barrier (Duan and Wei, 2013). Overall, there are no systematic biases between the model and data.

https://doi.org/10.5194/egusphere-2025-1229
Preprint. Discussion started: 13 May 2025

3.5.2 Northern Bering Sea (M8)

The model simulations also reproduce the observed seasonal and interannual variability of temperature and salinity profiles at the northern mooring M8 (Fig. 13). Here water property variability is related to sea ice, with 2018 being the warmest year throughout the water column and the year with the least ice extent (Fig. 7b). Prior to 2014, temperatures were colder both in the observations and in model simulations. The summer wind mixed layer at M8 is typically < 20 m (Stabeno et al., 2020), which is not observed since the top instrument was at ~20 m to avoid ice keels. The thermocline gradient is not as sharp at M8 as at M2 (Stabeno et al., 2012). The model replicates the penetration of heat below the mixed layer that is evident in the data. The seasonal mean vertical structure of temperature from the model are in excellent agreement with observations (Fig. S1 e-h).

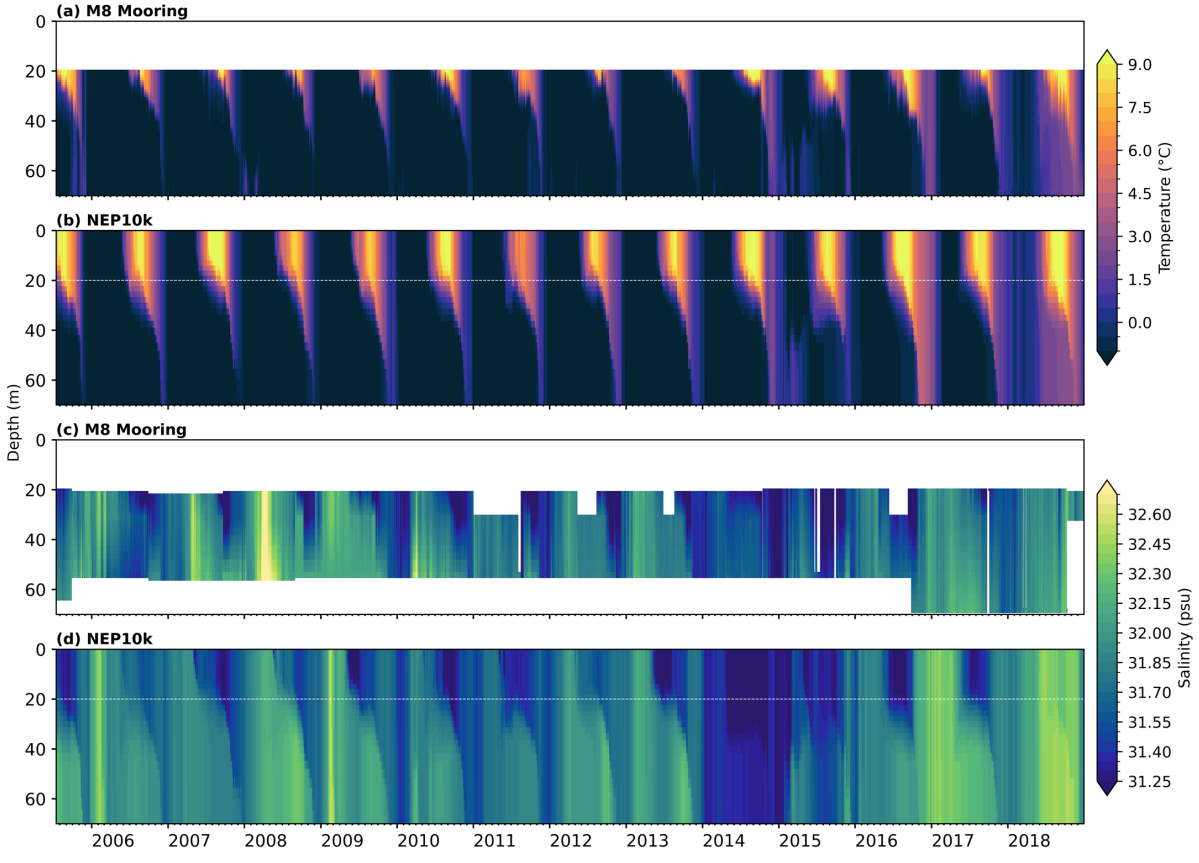

Figure 13: As in Fig. 12a-d, except for M8.

https://doi.org/10.5194/egusphere-2025-1229
Preprint. Discussion started: 13 May 2025

Salinity at M8 has a strong seasonal signal, with freshening occurring in the water column in fall, which is a result of mixing the fresh surface water downward, the fresh surface layer is a result of ice melt from the previous spring (2018 doesn't have this signal). Why 2014 is anomalously fresh in both OBS and model is unclear. The model did not capture the extreme salinity in 2008.

485

3.5.3 Surface and bottom temperatures

A more detailed statistical analysis was completed for the surface and bottom temperature at both moorings. The model replicates the annual signal both at the surface and at the bottom at M2 (Fig. 14 a, b) and at M8 (Fig. 15 a, b). The interannual variability is also captured at both sites (Figs. 14c,d and 15c,d), including the warm periods (2001-2005, 2014-2018) and the
490 cold period (2007-2013). Note that the near-surface temperature anomaly at M8 has less variability than at M2 because it is below the surface mixed layer during summer. At both locations, greater discrepancy between simulation and observation occurs at the near-bottom temperature after 2014, when the Bering Sea shelf shifted from cold to warmer conditions.

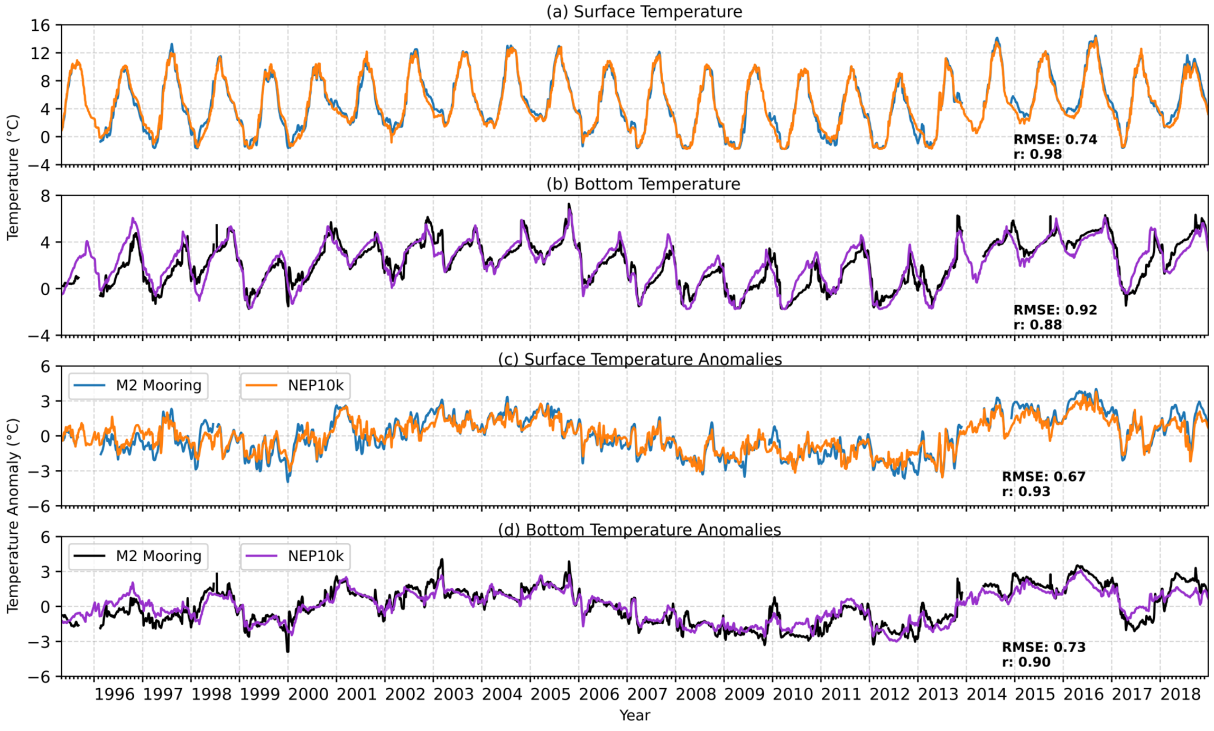

495

Figure 14: The time series at M2 of (a) near-surface and (b) near-bottom temperatures for model and observations (see panel (c) and (d) for line legends). Time series with the mean seasonal signal removed for: (c) near-surface temperature anomalies, and (d) near-bottom temperature anomalies. Correlation values are significant (p<0.001).

https://doi.org/10.5194/egusphere-2025-1229
Preprint. Discussion started: 13 May 2025

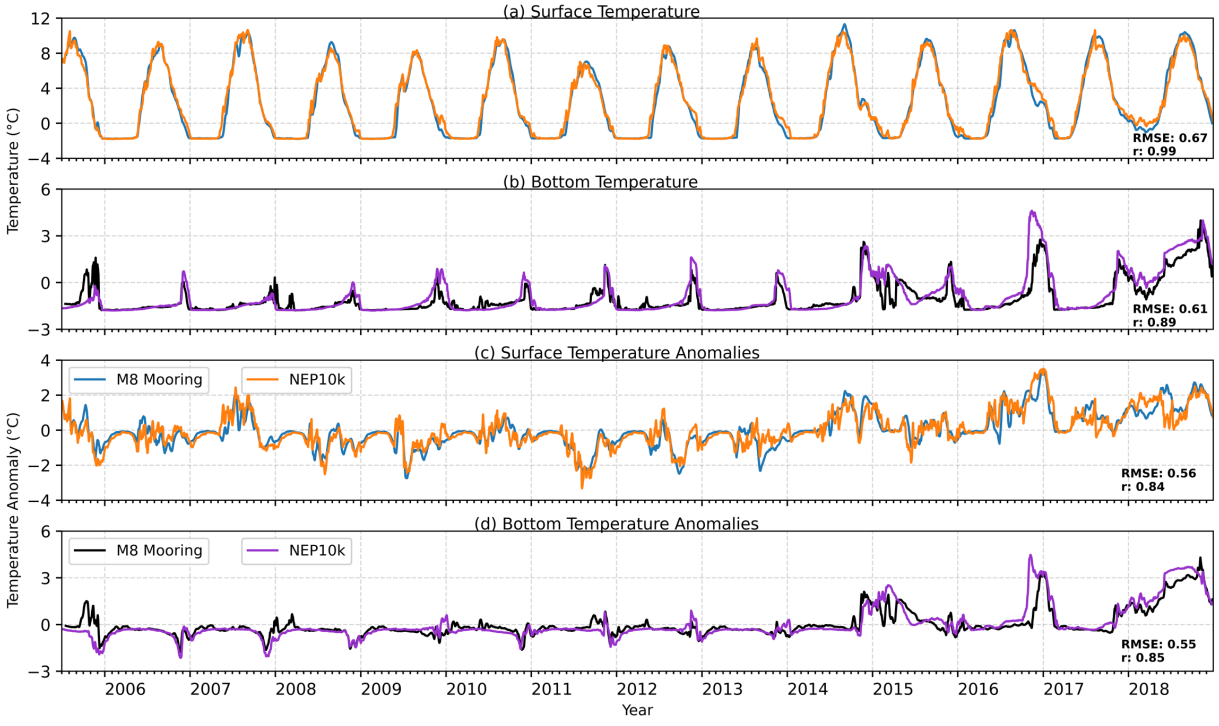

Figure 15: Same as in Fig. 14 except for M8.

Modeled bottom temperature is particularly sensitive to parameterized mixing schemes (Fig. 4) bottom temperature regulates distribution of several commercially important fish species.

3.6 Bering Sea cold pool

Summer and fall ocean temperature in the eastern Bering Sea is significantly impacted by seasonal sea ice that typically forms in the fall/winter and melts in late-winter or spring (Stabeno et al., 2012b). Most of the shelf region experiences colder temperatures in years with extensive sea-ice cover that lasts late into the ice season, and warmer temperatures in years with limited sea ice cover and/or early retreat. Temperature plays a significant role in thermal stratification, affecting the spatial structure of pelagic and demersal communities, the trophic structure of the Bering Sea food web and fish population demographics (Ladd and Stabeno, 2012; Spencer et al., 2016; Grüss et al., 2021). The "cold pool" refers to the cold water mass that persists near the bottom as a result of sea ice melting and insulation from the surface heating during the summer. Historically, it was defined as waters colder than 2°C, although other thresholds have been used. Both AFSC summer Bottom Trawl Survey and survey-replicated MOM6-NEP output show a southward extension of the cold pool along the middle shelf from the northwest to the southeast, while relatively warm temperature resides on the inner and outer shelves during summer

https://doi.org/10.5194/egusphere-2025-1229
Preprint. Discussion started: 13 May 2025

515 (Fig. 16 a, b). While the long-term model and observation means of summer cold pool are similar, Fig. 16c highlights areas of discrepancy. In general, the simulation has a modest warm bias in the shallow region and a cold bias near the continental slope.

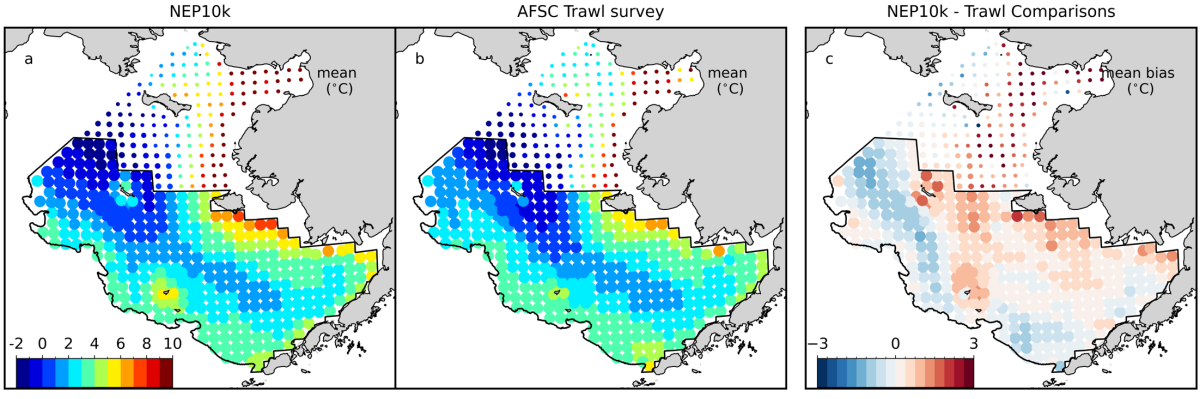

520 **Figure 16: A comparison of Bering Sea mean (1993-2018) bottom temperatures from (a) MOM6-NEP10K (subsampled to trawl survey locations and times) and (b) AFSC trawl survey measurements. (c) The differences between the modeled (a) and AFSC trawl survey (b).**

A range of cold-pool indices are defined by the proportion of the Bering Sea survey area with bottom temperatures colder than
525 2°C, 1°C, 0°C, and -1°C. The modeled and observed interannual cold-pool indices show remarkable agreement (Fig. 17), especially for the higher (> -1°C) temperature thresholds. Combined with the spatial patterns seen in Fig. 16, these results suggest that the model accurately represents the interannual variability and spatial extent of the cold pool. The ability of the model to replicate the cold pool dynamics is essential for understanding ecosystem dynamics and fisheries management applications.

530

https://doi.org/10.5194/egusphere-2025-1229
Preprint. Discussion started: 13 May 2025

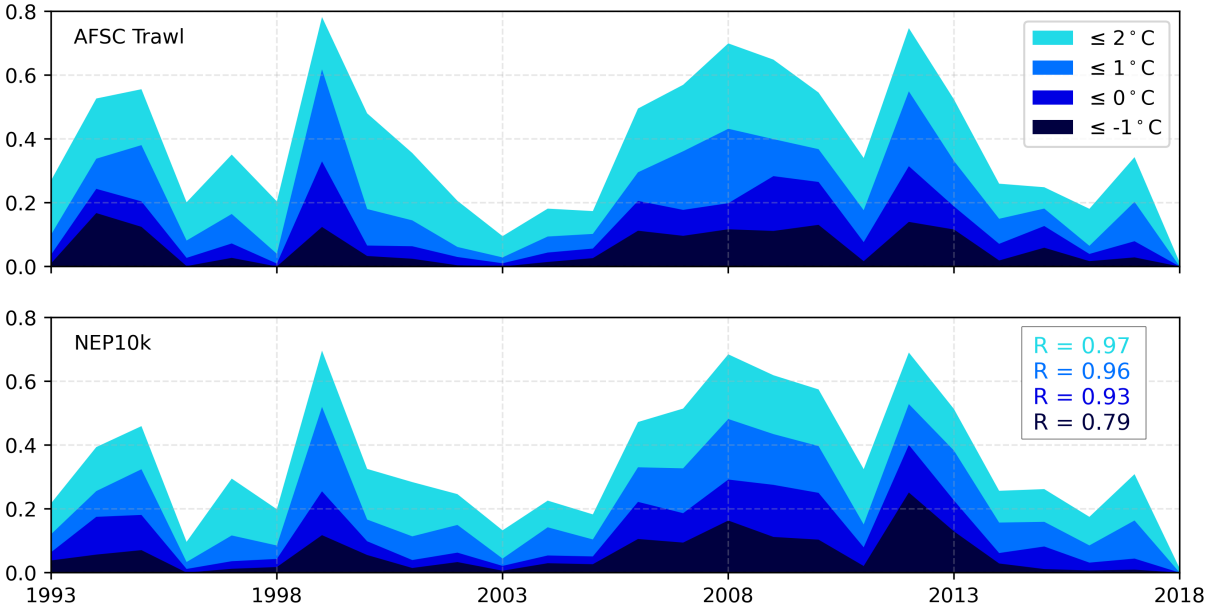

Figure 17: Cold pool indices defined as the proportion of the southeastern Bering Sea survey area (outlined by black line on Fig. 16) colder than four thresholds (2°C, 1°C, 0°C, and -1°C). These summer indices are (a) AFSC trawl survey and (b) MOM6-NEP10K during 1993–2018. Correlation between the modeled and measured cold pool indices are indicated on the bottom panel.

4 Conclusions and Discussion

MOM6 has long been used in global Earth System Model simulations (Held et al., 2019). Advantages of MOM6 include its more advanced sub-grid scale parameterizations and the ALE vertical coordinate, which allows for larger time steps and faster integration of the model. These features make MOM6 a powerful tool for accurately and efficiently modeling ocean conditions in the past and predicting changes in the future. On the other hand, application of MOM6 in the regional modeling framework is relatively new, and only a few studies have addressed its performance in the context of high-resolution regional modeling. In this study, we evaluated a coupled ocean-sea ice model MOM6-NEP hindcast simulation (1993-2018) against satellite and in-situ observations. This study complements results in Drenkard et al. (2024), where coast-wide (from Baja to Chukchi) evaluation under a different atmospheric reanalysis forcing is presented.

We found that the model captured the main near-surface ocean circulation features on the Bering Sea basin and on the shelf. The ability to capture the weak shelf circulation (e.g. flow along the 50-m and 100-m isobath) is an improvement over our previous Regional Ocean Modeling System (ROMS) based simulations at 10km resolution (Kearney et al., 2020) and references therein), where bathymetry was necessarily smoothed and flows followed the “f/H” contours too strongly, partly due to the pressure gradient errors inherent in terrain-following coordinate systems (Griffies and Treguier, 2013). Given that

https://doi.org/10.5194/egusphere-2025-1229
Preprint. Discussion started: 13 May 2025

the ocean's dynamics are so sensitive to the bathymetric contours, it is critical to include realistic bathymetric features and properly render cross-isobath flows.

The original MOM6 shear-driven mixing scheme (Jackson et al., 2008) over-mixed the water column in the bottom boundary layer, especially over the energetic tidally driven southern Bering Sea shelf. This over-mixing was improved when we introduced a new scaling factor to reduce the turbulence decay length scale. This result points to the need for improving the interactions among surface, bottom boundary layer and interior mixing schemes. With the new scaling factor, water mass properties over the Bering Sea shelf as measured by EcoFOCI biophysical moorings are well captured by the model simulation, and in particular, the MLD and the sharp thermocline along the middle domain in summer is well preserved in the model. MLD along the Bering Sea slope still shows significant deep biases. Improvements to the model as well as observational data could bring the model and data closer together.

Responding to, and driving water mass properties, the modeled sea ice over the Bering Sea shelf closely matches observations in terms of shelf-wide ice extent and its mean seasonal cycle and interannual variability, as well as sea-ice arrival and retreat timing in both the southern and northern shelf. This is also an improvement over prior ROMS Bering Sea simulations, where modeled sea-ice tended to arrive and melt later than observations by ~2 weeks (Kearney et al., 2020). Sea-ice seasonal timing is critical to the Bering Sea ecosystem dynamics. However, over the northern shelf, ice concentration during the late-April to May melt season tends to have reduced interannual variability - the simulation has smaller (larger) ice concentration in relatively cold (warm) periods than in observations. Sea-ice over the northern shelf is highly dynamic during the melting season. The exact reasons contributing to this discrepancy remain to be understood. Another area in need of future improvement is the open boundary conditions for limited domain sea-ice modeling. Currently, MOM6-NEP has closed ice lateral boundaries along its eastern and northern edges. These closed boundaries are found to degrade its performance on the Chukchi Sea shelf, where sea-ice accumulated along the boundaries where in reality they are advected across the boundaries (Dukovskoy, personnel communications). The closed ice boundaries do not appear to degrade the sea-ice simulation on the Bering Sea, where sea ice is mostly formed in situ instead of being advected in from the shallow and narrow Bering Strait.

We also investigated the Bering Sea cold pool in this study, as it plays an important role in ecosystem dynamics and is strongly influenced by seasonal sea ice. As evidenced by the agreement between AFSC trawl survey measurements and model simulations, the cold pool spatial and temporal variability is accurately replicated by the model, with a strong correlation for multiple temperature thresholds. While the model replicates the cold pool dynamics of the Bering Sea shelf where horizontal flow is weak, we also note the difference in cold pool indices between this study and Drenkard et al. (2024) (compare Fig. 17 with their Fig. 20). This is likely caused by the difference in the two atmospheric forcing products (JRA55 in this study versus ERA5 in (Drenkard et al., 2024). The uncertainties associated with different forcing data sets in regional ocean-sea ice modeling should be kept in mind when interpreting these modeling results.

https://doi.org/10.5194/egusphere-2025-1229
Preprint. Discussion started: 13 May 2025

In contrast to the middle shelf dynamics, there are some systematic biases between the model and trawl survey measurements near the continental slope and on the outer shelf (water depth 100 - 180 m) of the eastern Bering Sea. The outer shelf is a region where horizontal advection, including on-shelf flow, is often observed, especially in the deep canyons abutting the slope. The proper strength of simulated on-shelf flow in the canyons needs to be further examined.

Other near-term future work includes bringing the span of hindcast simulation closer to the present day and operationalizing its workflow. This is the first step towards building a reliable ocean modeling system capable of historical hindcasting, seasonal to interannual forecasting/prediction, and multi-decadal projections. Continued model improvements, data collection, and careful model evaluation will increase our understanding and confidence in using these modeling systems to support marine resource management decision making, which is the ultimate goal of CEFI.

Code availability

The source code of the model component has been archived at https://doi.org/10.5281/zenodo.15009640 (Seelanki et al., 2025a). The MOM6 is developed openly, and the GitHub repositories are located at https://github.com/mom-ocean/MOM6 and https://github.com/NOAA-GFDL/MOM6, respectively (last access: 11 September 2024). Other model component repositories are also accessible at https://github.com/NOAA-GFDL (last access: 11 September, 2024). These platforms allow users to download the most recent and experimental versions of the source code, report bugs, and contribute new features. Alaska Fisheries Science Center (AFSC) R code base used for the Bering Sea Cold Pool Analyses can be found on GitHub: https://github.com/afsc-gap-products/coldpool, which utilizes the AFSC akgfmaps toolset, also on GitHub: https://github.com/afsc-gap-products/akgfmaps.

Data availability

The model parameter, forcing, and initial condition files are available at https://doi.org/10.5281/zenodo.15009973 (Seelanki et al., 2025b). All model output that was analyzed in this study is available at https://doi.org/10.5281/zenodo.15009797 (Seelanki et al., 2025c). The datasets used for model forcing and validation are cited in the main text and listed in the Table 2, where the data can be downloaded are listed as follows: OISSTv2 (https://psl.noaa.gov/data/gridded/data.noaa.oisst.v2.highres.html, Huang et al., 2021); GLORYS12 reanalysis (https://doi.org/10.48670/moi-00021, Jean-Michel et al., 2021); JRA55-do version 1.5 (https://climate.mri-jma.go.jp/pub/ocean/JRA55-do/, Tsujino et al., 2018); NCEI Northern North Pacific Regional Climatology Version 2 (https://www.ncei.noaa.gov/products/northern-north-pacific-regional-climatology, Seidov et al., 2023); NASA NSIDC Sea Ice Concentrations (https://nsidc.org/data/nsidc-0079/versions/4 and https://nsidc.org/data/nsidc-0081/versions/2); Mixed

https://doi.org/10.5194/egusphere-2025-1229
Preprint. Discussion started: 13 May 2025

layer depth over the global ocean (https://doi.org/10.17882/98226 , de Boyer Montégut, 2024); Global Ocean Gridded L 4 Sea Surface Heights And Derived Variables (https://doi.org/10.48670/moi-00148, Mercator Ocean, 2021); TPXO9 (https://www.tpxo.net/home, Egbert and Erofeeva, 2002); GloFAS (https://doi.org/10.24381/cds.a4fdd6b9, Zsoter, 2021); AFSC bottom trawl gear temperature data (https://github.com/afsc-gap-products/coldpool/tree/main/data, Rohan et al., 2022); Eco-FOCI moorings data is available upon request from Margaret (Peggy) Sullivan (peggy.sullivan@noaa.gov).

Authors contributions

Conceptualization: VS, WC, PJS, AJH. Model configuration: VS, EJD, KH. Model simulations: VS. Formal analysis: VS. Model evaluation: VS, AJH, WC, PJS. Visualization: VS. Investigation: VS, WC, PJS, AJH. Supervision: WC, AJH, PJS. Funding acquisition: PJS, WC, AJH. Original draft: VS. Review and editing: VS, WC, PJS, AJH, EDJ, CAS, KH.

Competing interests

The authors declare that they have no conflict of interest

Acknowledgements

This publication is partially funded by CEFI, EcoFOCI, NOAA's Arctic Research programs, and NOAA Research and the Cooperative Institute for Climate, Ocean, and Ecosystem Studies (CICOES) under NOAA Cooperative Agreement NA20OAR4320271. The authors extend their thanks to Ryan McCabe for his valuable suggestions during the NOAA internal review process. We thank the captains, crews and scientists who participated in the deployment and recovery of the NOAA EcoFOCI moorings included in this paper. The statements, findings, conclusions, and recommendations are those of the authors and do not reflect the views of NOAA or the Department of Commerce. With this configuration, multi-decadal (1993-2018) ocean hindcast simulations were carried out on NOAA High-Performance Computing (HPC2) housed at Mississippi State University. This is NOAA PMEL Contribution #5738, EcoFOCI Contribution # EcoFOCI-1071.

https://doi.org/10.5194/egusphere-2025-1229
Preprint. Discussion started: 13 May 2025

References

Adcroft, A. and Campin, J.-M.: Rescaled height coordinates for accurate representation of free-surface flows in ocean circulation models, Ocean Model., 7, 269-284, https://doi.org/10.1016/j.ocemod.2003.09.003, 2004.

Adcroft, A., Anderson, W., Balaji, V., Blanton, C., Bushuk, M., Dufour, C. O., Dunne, J. P., Griffies, S. M., Hallberg, R., Harrison, M. J., Held, I. M., Jansen, M. F., John, J. G., Krasting, J. P., Langenhorst, A. R., Legg, S., Liang, Z., McHugh, C., Radhakrishnan, A., Reichl, B. G., Rosati, T., Samuels, B. L., Shao, A., Stouffer, R., Winton, M., Wittenberg, A. T., Xiang, B., Zadeh, N., and Zhang, R.: The GFDL Global Ocean and Sea Ice Model OM4.0: Model description and simulation features, J. Adv. Model. Earth Syst., 11, 3167-3211, https://doi.org/10.1029/2019MS001726, 2019.

Amaya, D. J., Alexander, M. A., Scott, J. D., and Jacox, M. G.: An evaluation of high-resolution ocean reanalyses in the California current system, Prog. Oceanogr., 210, 102951, https://doi.org/10.1016/j.pocean.2022.102951, 2023.

Arakawa, A. and Lamb, V. R.: Computational design of the basic dynamical processes of the UCLA General Circulation Model, Method Computat. Phy.-Adv. Res. Appl., 17, 173-265, https://doi.org/10.1016/B978-0-12-460817-7.50009-4, 1977.

Bleck, R.: An oceanic general circulation model framed in hybrid isopycnic-Cartesian coordinates, Ocean Model., 4, 55-88, https://doi.org/10.1016/S1463-5003(01)00012-9, 2002.

Bodner, A. S., Fox-Kemper, B., Johnson, L., Roekel, L. P. V., McWilliams, J. C., Sullivan, P. P., Hall, P. S., and Dong, J.: Modifying the mixed layer eddy parameterization to include frontogenesis arrest by boundary layer turbulence, J. Phys. Oceanogr., 53, 323–339, https://doi.org/10.1175/JPO-D-21-0297.1, 2023.

Buckley, T. W., Grieg, A., and Boldt, J. L.: Describing summer pelagic habitat over the continental shelf in the eastern Bering Sea, 1982-2006, NOAA Tech. Memo. NMFS-AFSC 196, US Dept. Commerce, 2009.

Castillo-Trujillo, A. C., Kwon, Y.-O., Fratantoni, P., Chen, K., Seo, H., Alexander, M. A., and Saba, V. S.: An evaluation of eight global ocean reanalyses for the Northeast U.S. Continental shelf, Prog. Oceanogr., 219, 103126, https://doi.org/10.1016/j.pocean.2023.103126, 2023.

Cheng, W., Curchitser, E., Ladd, C., Stabeno, P., and Wang, M.: Influences of sea ice on the Eastern Bering Sea: NCAR CESM simulations and comparison with observations, Deep Sea Res. Part II Top. Stud. Oceanogr., 109, 27-38, https://doi.org/10.1016/j.dsr2.2014.03.002, 2014.

Coachman, L. K.: Circulation, water masses, and fluxes on the southeastern Bering Sea shelf, Cont. Shelf Res., 5, 23-108, https://doi.org/10.1016/0278-4343(86)90011-7, 1986.

Cokelet, E. D. and Stabeno, P. J.: Mooring observations of the thermal structure, salinity, and currents in the SE Bering Sea basin, J. Geophys. Res. Oceans, 102, 22947-22964, https://doi.org/10.1029/97JC00881, 1997.

Cokelet, E. D., Schall, M. L., and Dougherty, D. M.: ADCP-referenced geostrophic circulation in the Bering Sea basin, J. Phys. Oceanogr., 26, 1113–1128, https://doi.org/10.1175/1520-0485(1996)026, 1996.

Danielson, S., Curchitser, E., Hedstrom, K., Weingartner, T., and Stabeno, P.: On ocean and sea ice modes of variability in the Bering Sea, J. Geophys. Res. Oceans, 116, C12034, https://doi.org/10.1029/2011JC007389, 2011.

https://doi.org/10.5194/egusphere-2025-1229
Preprint. Discussion started: 13 May 2025

de Boyer montégut, C.: Mixed layer depth over the global ocean: a climatology computed with a density threshold criterion of 0.03 kg/m3 from the value at the reference depth of 5 m, SEANOE [dataset], 10.17882/98226, 2024.

de Boyer montégut, C., Madec, G., Fischer, A. S., Lazar, A., and Iudicone, D.: Mixed layer depth over the global ocean: An examination of profile data and a profile-based climatology, Journal of Geophysical Research: Oceans, 109, C12003, https://doi.org/10.1029/2004JC002378, 2004.

Drenkard, E. J., Stock, C. A., Ross, A. C., Teng, Y.-C., Morrison, T., Cheng, W., Adcroft, A., Curchitser, E., Dussin, R., Hallberg, R., Hauri, C., Hedstrom, K., Hermann, A., Jacox, M. G., Kearney, K. A., Pages, R., Pilcher, D. J., Pozo Buil, M., Seelanki, V., and Zadeh, N.: A regional physical-biogeochemical ocean model for marine resource applications in the Northeast Pacific (MOM6-COBALT-NEP10k v1.0), Geosci. Model Dev. Discuss. [preprint], https://doi.org/10.5194/gmd-2024-195, 2024.

Duan, W. and Wei, C.: The 'spring predictability barrier' for ENSO predictions and its possible mechanism: results from a fully coupled model, Int. J. Climatol., 33, 1280-1292, https://doi.org/10.1002/joc.3513, 2013.

Egbert, G. D., and Erofeeva, S. Y.: Efficient inverse modeling of barotropic ocean tides, J. Atmos. Ocean. Tech., 19, 183-204, https://doi.org/10.1175/1520-0426(2002)019 <0183:EIMOBO>2.0.CO;2, 2002.

Flather, R. A.: A tidal model of the northwest European continental shelf, Mem. Soc. Roy. Sci. Liege, 10, 141-164, 1976.

Fox-Kemper, B., Danabasoglu, G., Ferrari, R., Griffies, S. M., Hallberg, R. W., Holland, M. M., Maltrud, M. E., Peacock, S., and Samuels, B. L.: Parameterization of mixed layer eddies. III: Implementation and impact in global ocean climate simulations, Ocean Model., 39, 61-78, https://doi.org/10.1016/j.ocemod.2010.09.002, 2011.

Frey, K. E., Moore, G. W. K., Cooper, L. W., and Grebmeier, J. M.: Divergent patterns of recent sea ice cover across the Bering, Chukchi, and Beaufort seas of the Pacific Arctic Region, Prog. Oceanogr., 136, 32-49, https://doi.org/10.1016/j.pocean.2015.05.009, 2015.

Griffies, S. M.: Elements of the modular ocean model (MOM), GFDL Ocean Group Tech. Rep, 7, 47, 2014.

Griffies, S. M. and Treguier, A. M.: Ocean circulation models and modeling, in: International Geophysics, vol. 103, edited by: Siedler, G., Griffies, S. M., Gould, J., and Church, J. A., Elsevier, 521-551, 2013.

Griffies, S. M., Adcroft, A., and Hallberg, R. W.: A primer on the vertical lagrangian-remap method in ocean models based on finite volume generalized vertical coordinates, J. Adv. Model. Earth Sy., 12, e2019MS001954, https://doi.org/10.1029/2019MS001954, 2020.

Grüss, A., Thorson, J. T., Stawitz, C. C., Reum, J. C. P., Rohan, S. K., and Barnes, C. L.: Synthesis of interannual variability in spatial demographic processes supports the strong influence of cold-pool extent on eastern Bering Sea walleye pollock (Gadus chalcogrammus), Prog. Oceanogr., 194, 102569, https://doi.org/10.1016/j.pocean.2021.102569, 2021.

Hallberg, R.: Stable split time stepping schemes for large-scale ocean modeling, J. Comput. Phys., 135, 54-65, https://doi.org/10.1006/jcph.1997.5734, 1997.

Hallberg, R. and Adcroft, A.: Reconciling estimates of the free surface height in Lagrangian vertical coordinate ocean models with mode-split time stepping, Ocean Model., 29, 15-26, https://doi.org/10.1016/j.ocemod.2009.02.008, 2009.

https://doi.org/10.5194/egusphere-2025-1229
Preprint. Discussion started: 13 May 2025

Held, I. M., Guo, H., Adcroft, A., Dunne, J. P., Horowitz, L. W., Krasting, J., Shevliakova, E., Winton, M., Zhao, M., Bushuk, M., Wittenberg, A. T., Wyman, B., Xiang, B., Zhang, R., Anderson, W., Balaji, V., Donner, L., Dunne, K., Durachta, J., Gauthier, P. P. G., Ginoux, P., Golaz, J.-C., Griffies, S. M., Hallberg, R., Harris, L., Harrison, M., Hurlin, W., John, J., Lin, P., Lin, S.-J., Malyshev, S., Menzel, R., Milly, P. C. D., Ming, Y., Naik, V., Paynter, D., Paulot, F., Ramaswamy, V., Reichl, B., Robinson, T., Rosati, A., Seman, C., Silvers, L. G., Underwood, S., and Zadeh, N.: Structure and Performance of GFDL's CM4.0 Climate Model, J. Adv. Model. Earth Sy., 11, 3691-3727, https://doi.org/10.1029/2019MS001829, 2019.

Huang, B., Liu, C., Banzon, V., Freeman, E., Graham, G., Hankins, B., Smith, T., Zhang, H.-M., Huang, B., Liu, C., Banzon, V., Freeman, E., Graham, G., Hankins, B., Smith, T., and Zhang, H.-M.: Improvements of the Daily Optimum Interpolation Sea Surface Temperature (DOISST) Version 2.1, J. Climate, 34, 2923–2939, https://doi.org/10.1175/JCLI-D-20-0166.1, 2021.

Hunke, E. C.: Sea ice volume and age: Sensitivity to physical parameterizations and thickness resolution in the CICE sea ice model, Ocean Model., 82, 45-59, https://doi.org/10.1016/j.ocemod.2014.08.001, 2014.

Hunt, G. L., Stabeno, P., Walters, G., Sinclair, E., Brodeur, R. D., Napp, J. M., and Bond, N. A.: Climate change and control of the southeastern Bering Sea pelagic ecosystem, Deep-Sea Res. Pt. II, 49, 5821-5853, https://doi.org/10.1016/S0967-0645(02)00321-1, 2002.

Hunt, G. L., Coyle, K. O., Eisner, L. B., Farley, E. V., Heintz, R. A., Mueter, F., Napp, J. M., Overland, J. E., Ressler, P. H., Salo, S., and Stabeno, P. J.: Climate impacts on eastern Bering Sea foodwebs: a synthesis of new data and an assessment of the Oscillating Control Hypothesis, ICES J. Mar. Sci., 68, 1230–1243, https://doi.org/10.1093/icesjms/fsr036, 2011.

Jackson, L., Hallberg, R., Legg, S., Jackson, L., Hallberg, R., and Legg, S.: A parameterization of shear-driven turbulence for ocean climate models, J. Phys. Oceanogr., 38, 1033–1053, https://doi.org/10.1175/2007JPO3779.1, 2008.

Jansen, M. F., Adcroft, A. J., Hallberg, R., and Held, I. M.: Parameterization of eddy fluxes based on a mesoscale energy budget, Ocean Model., 92, 28-41, https://doi.org/10.1016/j.ocemod.2015.05.007, 2015.

Jean-Michel, L., Eric, G., Romain, B.-B., Gilles, G., Angélique, M., Marie, D., Clément, B., Mathieu, H., Olivier, L. G., Charly, R., Tony, C., Charles-Emmanuel, T., Florent, G., Giovanni, R., Mounir, B., Yann, D., and Pierre-Yves, L. T.: The Copernicus Global 1/12° Oceanic and Sea Ice GLORYS12 Reanalysis, Front. Earth Sci., 9, 698876, https://doi.org/10.3389/feart.2021.698876, 2021.

Kearney, K.: Temperature Data from the Eastern Bering Sea Continental Shelf Bottom Trawl Survey as Used for Hydrodynamic Model Validation and Comparison, NOAA Technical Memorandum NMFS-AFSC-415, https://doi.org/10.25923/e77k-gg40, 2021.

Kearney, K., Hermann, A., Cheng, W., Ortiz, I., and Aydin, K.: A coupled pelagic–benthic–sympagic biogeochemical model for the Bering Sea: documentation and validation of the BESTNPZ model (v2019.08.23) within a high-resolution regional ocean model, Geosci. Model Dev., 13, 597–650, https://doi.org/10.5194/gmd-13-597-2020, 2020.

Kobayashi, S., Ota, Y., Harada, Y., Ebita, A., Moriya, M., Onoda, H., Onogi, K., Kamahori, H., Kobayashi, C., Endo, H., Miyaoka, K., and Takahashi, K.: The JRA-55 Reanalysis: General Specifications and Basic Characteristics, J. Meteorol. Soc. Jpn. Ser. II, 93, 5-48, https://doi.org/10.2151/jmsj.2015-001, 2015.

https://doi.org/10.5194/egusphere-2025-1229
Preprint. Discussion started: 13 May 2025

Ladd, C.: Seasonal and interannual variability of the Bering Slope Current, Deep -Sea Res. Pt. II, 109, 5-13, https://doi.org/10.1016/j.dsr2.2013.12.005, 2014.

Ladd, C. and Stabeno, P. J.: Stratification on the Eastern Bering Sea shelf revisited, Deep -Sea Res. Pt. II, 65-70, 72-83, https://doi.org/10.1016/j.dsr2.2012.02.009, 2012.

Large, W. G. and Yeager, S. G.: Diurnal to decadal global forcing for ocean and sea-ice models: The data sets and flux climatologies, NCAR/TN-460+STR, NCAR Technical Note, National Center for Atmospheric Research, https://doi.org/10.5065/D6KK98Q6, 2004.

Lauth, R. R.: Results of the 2010 eastern and northern Bering Sea continental shelf bottom trawl survey of groundfish and invertebrate fauna, NOAA Technical Memorandum NMFS-AFSC 227, 2011.

Manizza, M., Quéré, C. L., Watson, A. J., and Buitenhuis, E. T.: Bio-optical feedbacks among phytoplankton, upper ocean physics and sea-ice in a global model, Geophys. Res. Lett., 32, L05603, https://doi.org/10.1029/2004GL020778, 2005.

Marchesiello, P., McWilliams, J. C., and Shchepetkin, A.: Open boundary conditions for long-term integration of regional oceanic models, Ocean Model., 3, 1-20, https://doi.org/10.1016/S1463-5003(00)00013-5, 2001.

Mercator Ocean: Global Ocean Gridded L4 Sea Surface Heights and Derived Variables Reprocessed 1993-Ongoing, https://doi.org/10.48670/moi-00148, 2021.

Onishi, H. and Ohtani, K.: On seasonal and year to year variation in flow of the Alaskan stream in the central North Pacific, J. Oceanogr., 55, 597–608, https://doi.org/10.1023/A:1007840802296, 1999.

Orlanski, I.: A simple boundary condition for unbounded hyperbolic flows, J. Comput. Phys., 21, 251-269, https://doi.org/10.1016/0021-9991(76)90023-1, 1976.

Reed, R. and Stabeno, P.: The recent return of the Alaskan Stream to Near Strait, J. Mar. Res., 51(3), 515-527, https://doi.org/10.1357/0022240933224025, 1993.

Reed, R. K. and Stabeno, P. J.: The Aleutian North Slope Current., in: Dynamics of the Bering Sea: A Summary of Physical, Chemical, and Biological Characteristics, and a Synopsis of Research on the Bering Sea, edited by: Loughlin, T.R., and Ohtani, K., University of Alaska Sea Grant, AK-SG-99-03, North Pacific Marine Science Organization (PICES), 1999.

Reichl, B. G. and Hallberg, R.: A simplified energetics based planetary boundary layer (ePBL) approach for ocean climate simulations., Ocean Model., 132, 112-129, https://doi.org/10.1016/j.ocemod.2018.10.004, 2018.

Ross, A. C., Stock, C. A., Adcroft, A., Curchitser, E., Hallberg, R., Harrison, M. J., Hedstrom, K., Zadeh, N., Alexander, M., Chen, W., Drenkard, E. J., du Pontavice, H., Dussin, R., Gomez, F., John, J. G., Kang, D., Lavoie, D., Resplandy, L., Roobaert, A., Saba, V., Shin, S.-I., Siedlecki, S., and Simkins, J.: A high-resolution physical–biogeochemical model for marine resource applications in the northwest Atlantic (MOM6-COBALT-NWA12 v1.0), Geosci. Model Dev., 16, 6943–6985, https://doi.org/10.5194/gmd-16-6943-2023, 2023.

Seelanki, V., Cheng, W., Stabeno, P. J., Hermann, A. J., Drenkard, E. J., Stock, C. A., Hedstrom, K.: Model source code for "Evaluation of a coupled ocean and sea-ice model (MOM6-NEP10k) over the Bering Sea and its sensitivity to turbulence decay scales", Zenodo[code], https://doi.org/10.5281/zenodo.15009640, 2025a.

https://doi.org/10.5194/egusphere-2025-1229
Preprint. Discussion started: 13 May 2025

Seelanki, V., Cheng, W., Stabeno, P. J., Hermann, A. J., Drenkard, E. J., Stock, C. A., Hedstrom, K.: Model input for "Evaluation of a coupled ocean and sea-ice model (MOM6-NEP10k) over the Bering Sea and its sensitivity to turbulence decay scales", Zenodo [Data set], https://doi.org/10.5281/zenodo.15009973, 2025b.

Seelanki, V., Cheng, W., Stabeno, P. J., Hermann, A. J., Drenkard, E. J., Stock, C. A., Hedstrom, K.: Model output for "Evaluation of a coupled ocean and sea-ice model (MOM6-NEP10k) over the Bering Sea and its sensitivity to turbulence decay scales", Zenodo [Data set], https://doi.org/10.5281/zenodo.15009797, 2025c.

Seidov, D., Mishonov, A.V., Baranova, O.K., Boyer, T.P., Nyadjro, E., Bouchard, C., and Cross, S.L.: Northwest Atlantic Regional Ocean climatology version 2. (NCEI Accession 0283566), NOAA National Centers for Environmental Information [dataset], https://doi.org/10.25921/dym6-q737, 2023.

Spencer, P. D., Holsman, K. K., Zador, S., Bond, N. A., Mueter, F. J., Hollowed, A. B., and Ianelli, J. N.: Modelling spatially dependent predation mortality of eastern Bering Sea walleye pollock, and its implications for stock dynamics under future climate scenarios, ICES J. Mar. Sci., 73, 1330–1342, https://doi.org/10.1093/icesjms/fsw040, 2016.

Stabeno, P., Napp, J., Mordy, C., and Whitledge, T.: Factors influencing physical structure and lower trophic levels of the eastern Bering Sea shelf in 2005: Sea ice, tides and winds, Prog. Oceanogr., 85, 180-196, https://doi.org/10.1016/j.pocean.2010.02.010, 2010.

Stabeno, P. J.: The physical oceanography of the Bering Sea, in: Dynamics of the Bering Sea: A Summary of Physical, Chemical, and Biological Characteristics, and a Synopsis of Research on the Bering Sea, edited by Loughlin, T.R. and Ohtani, K., North Pacific Marine Science Organization (PICES), University of Alaska Sea Grant, AK-SG-99-03, 1–28, 1999.

Stabeno, P. J. and Bell, S. W.: Extreme conditions in the Bering Sea (2017–2018): Record-breaking low sea-ice extent, Geophys. Res. Lett., 46, 8952-8959, https://doi.org/10.1029/2019GL083816, 2019.

Stabeno, P. J. and Hristova, H. G.: Observations of the Alaskan Stream near Samalga Pass and its connection to the Bering Sea: 2001–2004, Deep-Sea Res. Pt. I, 88, 30-46, https://doi.org/10.1016/j.dsr.2014.03.002, 2014.

Stabeno, P. J. and Reed, R. K.: Circulation in the Bering Sea basin observed by satellite-tracked drifters: 1986–1993, J. Phys. Oceanogr., 24, 848–854, https://doi.org/10.1175/1520-0485(1994)024 <0848:CITBSB>2.0.CO;2, 1994.

Stabeno, P. J., Ladd, C., and Reed, R. K.: Observations of the Aleutian North Slope Current, Bering Sea, 1996–2001, J. Geophys. Res. Oceans, 114, C05015, https://doi.org/10.1029/2007JC004705, 2009.

Stabeno, P. J., Mordy, C. W., and Sigler, M. F.: Seasonal patterns of near-bottom chlorophyll fluorescence in the eastern Chukchi Sea: 2010–2019, Deep-Sea Res. Pt. II, 177, 104842, https://doi.org/10.1016/j.dsr2.2020.104842, 2020.

Stabeno, P. J., Reed, R. K., and Overland, J. E.: Lagrangian measurements in the Kamchatka Current and Oyashio, J. Oceanography, 50653–662, https://doi.org/10.1007/BF02270498, 1994.

Stabeno, P. J., Kachel, D. G., Kachel, N. B., and Sullivan, M. E.: Observations from moorings in the Aleutian Passes: temperature, salinity and transport, Fish. Oceanogr., 14, 39-54, https://doi.org/10.1111/j.1365-2419.2005.00362.x, 2005.

https://doi.org/10.5194/egusphere-2025-1229
Preprint. Discussion started: 13 May 2025

Stabeno, P. J., Bell, S., Berchok, C., Cokelet, E. D., Cross, J., McCabe, R. M., Mordy, C. W., Overland, J., Strausz, D., Sullivan, M., and Tabisola, H. M.: Long-term biophysical observations and climate impacts in US Arctic marine ecosystems, Oceanography, 36, 78–85, https://doi.org/10.5670/oceanog.2023.225, 2023.

Stabeno, P. J., Danielson, S. L., Kachel, D. G., Kachel, N. B., and Mordy, C. W.: Currents and transport on the Eastern Bering Sea shelf: An integration of over 20 years of data, Deep-Sea Res. Pt. II, 134, 13-29, https://doi.org/10.1016/j.dsr2.2016.05.010, 2016.

Stabeno, P. J., Kachel, N. B., Moore, S. E., Napp, J. M., Sigler, M., Yamaguchi, A., and Zerbini, A. N.: Comparison of warm and cold years on the southeastern Bering Sea shelf and some implications for the ecosystem, Deep-Sea Res. Pt. II, 65-70, 31-45, https://doi.org/10.1016/j.dsr2.2012.02.020, 2012b.

Stabeno, P. J., Farley Jr., E. V., Kachel, N. B., Moore, S., Mordy, C. W., Napp, J. M., Overland, J. E., Pinchuk, A. I., and Sigler, M. F.: A comparison of the physics of the northern and southern shelves of the eastern Bering Sea and some implications for the ecosystem, Deep-Sea Res. Pt. II, 65-70, 14-30, https://doi.org/10.1016/j.dsr2.2012.02.019, 2012.

Stalin, S., Bell, S., Delich, N., Mordy, C. W., and Stabeno, P. J.: Advancing observational infrastructure in the Arctic, Oceanography, 36, 86–87, https://doi.org/10.5670/oceanog.2023.227, 2023.

Tsujino, H., Urakawa, S., Nakano, H., Small, R. J., Kim, W. M., Yeager, S. G., Danabasoglu, G., Suzuki, T., Bamber, J. L., Bentsen, M., Böning, C. W., Bozec, A., Chassignet, E. P., Curchitser, E., Dias, F. B., Durack, P. J., Griffies, S. M., Harada, Y., Ilicak, M., Josey, S. A., and Yamazaki, D.: JRA-55 based surface dataset for driving ocean–sea-ice models (JRA55-do), Ocean Model., 130, 79-139, https://doi.org/10.1016/j.ocemod.2018.07.002, 2018.

Wang, J., Hu, H., Mizobata, K., and Saitoh, S.-i.: Seasonal variations of sea ice and ocean circulation in the Bering Sea: A model-data fusion study, J. Geophys. Res. Oceans, 114, C02011, https://doi.org/10.1029/2008JC004727, 2009.

Wang, J., Hu, H., Goes, J., Miksis-Olds, J., Mouw, C., D'Sa, E., Gomes, H., Wang, D. R., Mizobata, K., Saitoh, S.-i., and Luo, L.: A modeling study of seasonal variations of sea ice and plankton in the Bering and Chukchi Seas during 2007–2008, J. Geophys. Res. Oceans, 118, 1520-1533, https://doi.org/10.1029/2012JC008322, 2013.

Woodgate, R. A., Aagaard, K., and Weingartner, T. J.: Interannual changes in the Bering Strait fluxes of volume, heat and freshwater between 1991 and 2004, Geophys. Res. Lett., 33, L15609, https://doi.org/10.1029/2006GL026931, 2006.

Woodgate, R. A., Weingartner, T., and Lindsay, R.: The 2007 Bering Strait oceanic heat flux and anomalous Arctic sea-ice retreat, Geophys. Res. Lett., 37, L01602, https://doi.org/10.1029/2009GL041621, 2010.

Woodgate, R. A., Weingartner, T. J., and Lindsay, R.: Observed increases in Bering Strait oceanic fluxes from the Pacific to the Arctic from 2001 to 2011 and their impacts on the Arctic Ocean water column, Geophys. Res. Lett., 39, L24603, https://doi.org/10.1029/2012GL054092, 2012.

Zhang, J., Woodgate, R., Moritz, R., Zhang, J., Woodgate, R., and Moritz, R.: Sea ice response to atmospheric and oceanic forcing in the Bering Sea, J. Phys. Oceanogr., 40, 1729–1747, https://doi.org/10.1175/2010JPO4323.1, 2010.

https://doi.org/10.5194/egusphere-2025-1229
Preprint. Discussion started: 13 May 2025

Zhuang, J., Dussin, R., Huard, D., Bourgault, P., Banihirwe, A., Raynaud, S., Malevich, B., Schupfner, M., Filipe, Levang, S., Gauthier, C., Jüling, A., Almansi, M., RichardScottOZ, RondeauG, Rasp, S., Smith, T. J., Stachelek, J., Plough, M., Pierre, Bell, R., Caneill, R., and Li, X.: pangeo-data/xESMF: v0.8.2 [dataset], https://doi.org/10.5281/zenodo.8356796, 2023.

Zsoter, E., Harrigan, S., Barnard, C., Wetterhall, F., Ferrario, I., Mazzetti, C., Alfieri, L., Salamon, P., Prudhomme, C: River discharge and related historical data from the Global Flood Awareness System, v3.1. European Commission, Joint Research Centre (JRC) [dataset], https://doi.org/10.24381/cds.a4fdd6b9, 2021.